Journal of Geophysical Research: Oceans

RESEARCH ARTICLE
10.1029/2018JC014177

Drivers of Antarctic Sea Ice Volume Change in CMIP5 Models

S. Schroeter[1,2,3], W. Hobbs[2,4], N. L. Bindoff[1,2,4,5], R. Massom[2,6], and R. Matear[5]

[1]Institute for Marine and Antarctic Studies, University of Tasmania, Hobart, Tasmania, Australia, [2]Antarctic Climate and Ecosystems Cooperative Research Centre (ACE CRC), Hobart, Tasmania, Australia, [3]ARC Centre of Excellence for Climate System Science (ARCCSS), Hobart, Tasmania, Australia, [4]ARC Centre of Excellence for Climate Extremes (ARCCLEX), Hobart, Tasmania, Australia, [5]CSIRO Oceans and Atmosphere, Hobart, Tasmania, Australia, [6]Australian Antarctic Division, Kingston, Tasmania, Australia

Abstract Antarctic sea ice trends have to date been linked to surface winds, through sea ice motion and atmospheric thermal advection. This paper analyzes sea ice volume in 10 Coupled Model Intercomparison Project Phase 5 (CMIP5) model configurations under pre-industrial and historical climate forcings, to compare the relative importance of ice motion and thermodynamic processes. We find that the models' responses to historical forcings is dependent on their sea ice motion formulation; models with low-magnitude sea ice motion tend to have historical trends that are dominated by thermodynamic processes, while sea ice models with higher-magnitude motion have more spatially variable relative contributions from dynamic and thermodynamic processes. Trends at the sea ice edge during the season of sea ice advance are generally dominated by dynamic processes, whereas during retreat thermodynamic trends dominate. The models show more disagreement in the sea ice interior. This analysis highlights the different estimates and patterns of sea ice volume among global climate models and offers insight into the drivers of sea ice volume change as well as the subsequent implications for simulated atmosphere-sea ice-ocean interactions.

Plain Language Summary Increasing observed Antarctic sea ice is thought to be largely driven by surface winds, through driving sea ice motion and advecting warm air southward to melt ice in some regions. However, global climate models do not reproduce observed sea ice trends. This paper analyzes the sea ice volume budget in 10 climate models to see how much simulated sea ice change is driven by dynamic processes such as wind-driven sea ice motion, and how much is due to thermodynamic freeze and melt processes. We find that the models generally agree when it comes to mean sea ice volume change, with dynamic processes dominating the sea ice edge and thermodynamic processes dominating in the interior of the sea ice pack. However, the models disagree about trends of sea ice volume. In the sea ice interior, each process dominates approximately half the models in all sea ice sectors, and thermodynamic processes tend to dominate in models with low-magnitude average sea ice motion. These results provide insight into the estimates and patterns of Antarctic sea ice in global climate models, helping to understand the disparity between simulated and observed sea ice trends.

Key Points:
- Thermodynamic drivers tend to dominate trends of Antarctic sea ice volume in models with low-magnitude mean sea ice mass transport
- Drivers of sea ice volume trends in models with higher-magnitude mean sea ice mass transport have large spatial and seasonal variability
- Biases in mean Antarctic sea ice concentration are unrelated to the dominant processes driving sea ice volume trends

Supporting Information:
- Supporting Information S1

Correspondence to:
S. Schroeter,
serena.schroeter@utas.edu.au

Citation:
Schroeter, S., Hobbs, W., Bindoff, N. L., Massom, R., & Matear, R. (2018). Drivers of Antarctic sea ice volume change in CMIP5 models. *Journal of Geophysical Research: Oceans, 123*, 7914–7938. https://doi.org/10.1029/2018JC014177

Received 15 MAY 2018
Accepted 20 SEP 2018
Accepted article online 27 SEP 2018
Published online 7 NOV 2018

1. Introduction

An overall increase of ~1.73% per decade between 1979 and 2015 in observed annual Antarctic sea ice extent masks large contrasting regional trends that almost cancel each other out, most notably a 4.5% per decade increase in the Ross Sea and a −2.6% per decade decrease in the Amundsen-Bellingshausen Sea (Comiso et al., 2017). Trends of Antarctic sea ice also vary seasonally, with the largest-magnitude trends during summer and autumn (Hobbs et al., 2016), though autumn concentration trends have been linked to changes in the spring (Holland, 2014). In autumn, total sea ice extent increased by 3.8% per decade over 1979–2015 compared with a 0.9% per decade increase during spring (Comiso et al., 2017).

Studies of Antarctic sea ice distribution have demonstrated both regional and seasonal heterogeneity in the sea ice response to atmospheric variability, with some sectors exhibiting the strong influence of a large-scale pattern of atmospheric variability while others do not. The lack of a strong large-scale atmospheric influence indicates either a sea ice response to atmospheric variability unexplained by the major modes, or a sea ice response to ocean processes (Matear et al., 2015; Raphael & Hobbs, 2014; Schroeter et al., 2017). Holland and Kwok (2012) found that observed trends in sea ice concentration were largely driven by surface winds; around most of West Antarctica, wind trends affected sea ice through wind-driven sea ice transport, while around East Antarctica, southward advection of warm air dominated sea

ice trends. It has been argued that autumn sea ice trends in some sectors (such as parts of the Amundsen-Bellingshausen Sea and the inner Ross Sea) are a delayed ocean response to wind changes altering sea ice motion and melt in the preceding spring (Holland, 2014). However, ocean heat contributes at least 50% of the energy required for the springtime Antarctic sea ice retreat (Gordon, 1981), and in models, the sea ice-atmosphere interactions are weaker during spring (Schroeter et al., 2017). It remains uncertain as to exactly how the ocean-sea ice-atmosphere exchange during spring affects the overall observed increase in Antarctic sea ice extent since 1979.

While the ensemble mean of a small number of global climate models in the Coupled Model Intercomparison Project Phase 5 (CMIP5) produces positive trends in sea ice extent, and other models have individual ensemble members that do likewise, the majority of CMIP5 models produce decreasing sea ice trends between 1979 and 2005 (Mahlstein et al., 2013; Shu et al., 2015; Turner et al., 2013; Zunz et al., 2013). Furthermore, the models generally do not reproduce the contrasting trends of sea ice concentration and extent observed in the satellite data over the Ross and Bellingshausen Seas (Hobbs et al., 2015, 2016; Turner et al., 2013), nor the seasonality of observed sea ice trends. The reasons for the disparity between observed and modeled sea ice trends are yet to be fully understood, though some model ocean and atmosphere deficiencies that can affect sea ice have been identified (National Academies of Sciences, Engineering, and Medicine, 2017). For example, simulations of both the mean state and trends of mean sea level pressure and surface winds in CMIP5 models generally show poor representation of several key atmospheric features. The atmosphere's zonal asymmetry (i.e., departures from the zonal mean circulation) is poorly reproduced by most models, both in terms of the mean state and variance (Haumann et al., 2014; Hosking et al., 2013). Biases in the representation of large-scale atmospheric variability in CMIP5 models indicate a poor representation of mean surface climate (and hence sea ice) in West Antarctica in particular, where the largest observed sea ice trends occur. The forced trend in CMIP5 models is highly dependent on the mean state, such that models with a positive bias in sea ice cover tend to have larger decreases in response to anthropogenic forcing (Bracegirdle et al., 2015).

The motivation of this study is to determine the relative contribution of dynamic and thermodynamic processes in driving simulated Antarctic sea ice changes and also how these drivers vary spatially and seasonally throughout the sea ice zone. The dynamic and thermodynamic drivers of sea ice change are intrinsically linked. Poleward flow of warm air from lower to higher latitudes both reduces sea ice formation and dynamically advects sea ice southward, to reduce overall sea ice extent; the reverse is true for equatorward airflow (Massom et al., 2008). Due to the constraints of the satellite record, observational studies of sea ice dynamics are restricted to the use of sea ice concentration and sea ice motion data (Holland, 2014; Holland & Kimura, 2016; Holland & Kwok, 2012); however, global coupled climate models have the advantage of outputting sea ice thickness as well as sea ice concentration data, enabling examination of sea ice volume and the calculation of a sea ice budget. The advantage of sea ice volume in climate models is that it allows a separation of dynamic and thermodynamic processes, with the underlying caveat that these processes remain closely linked as described above. Without an equivalent large-scale continuous observational data set of sea ice thickness, however, validation of model output against observations is limited, thus highlighting the need for improved satellite observations of sea ice motion and thickness (National Academies of Sciences, Engineering, and Medicine, 2017).

In this study, we investigate dynamic and thermodynamic contributions to the sea ice volume budget in global coupled climate models with different mean states and trends in Antarctic sea ice, by decomposing modeled sea ice budgets into advective and thermodynamic freeze/melt components. Although it has been suggested that detailed analyses of sea ice drivers and processes in individual models are warranted to identify the origins of model biases (Lecomte et al., 2016), there have been few such intermodel comparisons of sea ice advective and thermodynamic changes. Previous model studies have examined only sea ice concentration, not the entire sea ice budget. These few studies, however, have yielded valuable insights into the behavior of simulated sea ice. For example, Uotila et al. (2014) demonstrated that the mean state of the Australian Community Climate and Earth System Simulator (ACCESS)-Ocean Model, the ocean and sea ice component of global coupled climate models ACCESS1-0 and ACCESS1-3 (among the better performing CMIP5 models with regard to Antarctic sea ice), overestimates sea ice motion at the coastline and the ice edge, resulting in an imbalance of the sea ice concentration budget compared with observations. The Max Planck Institute Earth System Low-Resolution model (MPI-ESM-LR), on the other

Table 1
Summary of Models From the Coupled Model Intercomparison Project Phase 5 (CMIP5) Used in This Study

Modeling Centre/group	Country	Model name	Historical ensembles	Horizontal resolution of sea ice	Sea ice model	Ocean model	Atmosphere model	Land model
Commonwealth Scientific and Industrial Research Organization and Australian Bureau of Meteorology	Australia	ACCESS1.0 (Bi et al., 2013)	3	300 × 360	CICE	MOM4	Unified Model ACGM	MOSES2 CABLE1.0
		ACCESS1.3 (Bi et al., 2013)						
Centre National de Recherches Météorologiques-Groupe d'études de l'Atmosphère Météorologique (CNRM-GAME) and the Centre Européen de Recherche et de Formation Avancée	France	CNRM-CM5 (Voldoire et al., 2013)	10	292 × 362	GELATO	NEMO	ARPEGE-Climate	SURFEX
NOAA Geophysical Fluid Dynamics Laboratory	United States	GFDL-CM3 (Griffies et al., 2011)	5	360 × 200	SIS	MOM4	AM3	LM3
Institut Pierre Simon Laplace	France	IPSL-CM5A-LR (Dufresne et al., 2013)	6	149 × 182	LIM2	ORCA2	LMDZ4	ORCHIDEE
		IPSL-CM5A-MR (Dufresne et al., 2013)	3					
Max-Planck-Institut für Meteorologie	Germany	MPI-ESM-LR (Jungclaus et al., 2013)	3	220 × 256	MPIOM	MPIOM	ECHAM6	JSBACH
		MPI-ESM-MR (Jungclaus et al., 2013)		404 × 802				
Meteorological Research Institute	Japan	MRI-CGCM3 (Yukimoto et al., 2012)	5	368 × 360	MRI.COM3	MRI.COM3	GSMUV	HAL
Norwegian Climate Centre	Norway	NorESM1-M (Bentsen et al., 2012)	3	384 × 320	CICE	MICOM	CAM-Oslo	CLM

hand, has an Antarctic sea ice concentration output that disagrees more strongly with observations. In this model, the dynamic influence of strengthening westerly winds may cause increased upwelling of warmer subsurface water and an enhanced thermodynamic response in the simulated sea ice (Haumann et al., 2014). A study of sea ice concentration in the Community Climate System Model and Institut Pierre Simon Laplace Low-Resolution model (IPSL-CM5A-LR), alongside an ocean-sea ice model forced by reanalysis winds, showed that mean errors in the central and outer sea ice pack are largely due to inadequate representation of wind strength and velocity, while errors in simulated sea ice near the coast may be equally influenced by the model ice rheology (Lecomte et al., 2016). Overestimated and underestimated Antarctic sea ice transport in global coupled climate models has substantial implications for trends of freshening or salinification of the ocean surface and stratification of the ocean column, with further consequences for the simulation of deep water properties and mode water formation to the north (Abernathey et al., 2016; Bitz et al., 2006; Haumann et al., 2016).

2. Data and Methods

Ten model configurations from the CMIP5 (Taylor et al., 2012) were chosen encompassing a range of sea ice, ocean, and atmosphere components, to obtain a representative sample of mean sea ice and forced sea ice responses. Details of the models used are given in Table 1. We restrict the analysis to 10 coupled models based on their different physics and sea ice trend patterns, to permit a more detailed analysis than would be practical for the entire CMIP5 suite (which numbers more than 40 models), while still including a broad range of model behaviors. Some models have very small differences in configuration, such as a different cloud physics scheme between ACCESS1-0 and ACCESS1-3 or different grid resolution between MPI-ESM-LR and MPI-ESM-MR; in these cases, examination of both models highlights the differences in their sea ice budgets that arise from these differing configurations. The differing mean states of sea ice in the models selected for this study, and some known biases contributing to these differences, are detailed in section 3.1.

We used pre-industrial control (piControl) and historical simulations, obtained from the multimodel archive at the Program for Climate Model Diagnosis and Intercomparison (Taylor et al., 2009, 2012), for monthly surface meridional and zonal winds (m/s), sea ice concentration, sea ice thickness (m), and sea ice transport (kg/s) along the *X* and *Y* direction of the native model grids. The piControl experiment is forced only by a time-invariant annual solar cycle and demonstrates the internal variability and mean state of variables in the model, while the historical experiment runs generally between 1850 and 2005 and is forced by realistic anthropogenic and natural climate forcings (Taylor et al., 2012). While in this paper we use piControl data to investigate the climatology of the variables, we do not explicitly investigate the interannual variability of the piControl simulations; this is an avenue for further investigation. All model variables were regridded onto a 1° latitude × 1° longitude grid for the budget calculation to rotate sea ice transport from along the *x* and *y* directions of the native grid cell to zonal and meridional transport, with regridded values being checked against native values to ensure consistency. To compare observed and simulated mean and trends of sea ice and surface winds, monthly sea ice concentration data for the period January 1979 to December 2005 were obtained from the National Snow and Ice Data Center (Meier et al., 2015), and monthly 10-m zonal and meridional wind data were obtained from the European Centre for Medium-Range Weather Forecasts (available at http://apps.ecmwf.int/). National Snow and Ice Data Center data were regridded from the 25-km × 25-km monthly Goddard-merged sea ice concentration product onto a 1° latitude × 1° longitude grid.

Our method is similar to that used by Holland and Kwok (2012); however, in this analysis, we are able to compute the total sea ice volume change rather than just sea ice concentration since the CMIP5 models also produce sea ice thickness data. This approach has some distinct advantages because the sea ice volume budget can be interpreted to mean that the "growth" term is due to thermodynamic freeze/melt (including ice growth by snow-driven flooding), whereas in Holland and Kwok (2012), internal dynamic processes leading to ice thickness change (such as ridging) could not be computed.

In equation (1), the left-hand side is the local change in sea ice volume (V), the first term on the right-hand side is the contribution from sea ice dynamics (advection and convergence) where $\mathbf{u}$ is the sea ice motion vector, and f is the tendency due to thermodynamic processes (freezing and melting), which we calculate as the residual of the first and second terms:

$$\frac{\partial V}{\partial t} = -\nabla\cdot(\mathbf{u}V) + f \tag{1}$$

Sea ice volume (V) is the product of sea ice concentration and thickness multiplied by the area of the grid cell. As all 10 CMIP5 models examined here have V centered at time step t, the center of the difference is at $t_{-1/2}$, which does not correspond to the time step of the sea ice dynamics term where the difference is at time step t (described below). To align these terms, $\partial V/\partial t$ was calculated through a central finite difference in time and is therefore the change averaged over the course of a time step, and not from one time step to the next.

The sea ice volume change (i.e., the left-hand side of equation (1)) was then calculated over each monthly time step in seconds (equation (1)), producing units of cubic meters per second:

$$\frac{\partial V}{\partial t} = \frac{\partial}{\partial t}\iint C\ T\ \mathrm{d}x\ \mathrm{d}y \tag{2}$$

where C is the grid cell sea ice concentration, T is sea ice thickness, and x and y are the grid cell zonal and meridional dimensions (m). The sea ice dynamics term (i.e., the first term on the right-hand side of equation (1)) was computed from the piControl and individual historical simulations. This term used the sea ice mass transport variables TRANSIX and TRANSIY (kg/s) as the spatial central finite difference across the x (for TRANSIX) and y (for TRANSIY) directions of each regridded cell and divided by a density constant (ρ) of 919 kg/m^3 (Timco & Frederking, 1996) to convert mass transport to sea ice volume transport (m^3/s). The sum of the x and y central finite differences produce the total divergence (i.e., the amount of output vs. input) of sea ice transport for each cell at each time step, denoting the sea ice volume tendency due to ice dynamics (whether the volume of sea ice transported into a grid cell is greater or less than the volume transported out). Unlike previous analyses, in which dynamics are separated into divergence ($C\nabla\cdot\mathbf{u}$) and advection ($\mathbf{u}\cdot\nabla C$) of the concentration terms (Holland & Kwok, 2012; Uotila et al., 2014), our calculations consider only the total divergence as the dynamic contribution to sea ice volume change, since our aim here was solely to compare the relative importance of the dynamic and thermodynamic contributions.

Casting equation (1) in terms of the discretized CMIP5 output variables, for a given model grid cell with western and eastern bounds (x_1,x_2) and southern/northern bounds (y_1,y_2), gives

$$\frac{\partial V}{\partial t} = -\left[\frac{(\mathrm{TRANSIX}(x_2) - \mathrm{TRANSIX}(x_1)) + (\mathrm{TRANSIY}(y_2) - \mathrm{TRANSIY}(y_1))}{\rho}\right] + f \tag{3}$$

The residual term is interpreted as thermodynamic change from both atmospheric and oceanic sources (Lecomte et al., 2016; Uotila et al., 2014). All three terms were then divided by the individual grid cell area and multiplied by the number of seconds in a year to give units of meters per year. Converting the units in this manner eliminates the effect of different grid cell areas due to the convergence of meridians at the poles.

Figure 1 shows the mean sea ice volume budget in the ACCESS1-0 model during the season of sea ice advance (March–August inclusive). The overall change in sea ice volume ($\partial V/\partial t$) is the sum of the two components: the sea ice dynamics term, indicating overall sea ice transport (equation (3)), and thermodynamic freeze/melt as discussed above. Blue shading in Figure 1a indicates an increase in sea ice volume over time ($\partial V/\partial t$). The dynamic term (Figure 1b) is positive at the sea ice edge (contributing toward the sea ice increase, suggesting northward advection) and negative along the coastline (diminishing the sea ice

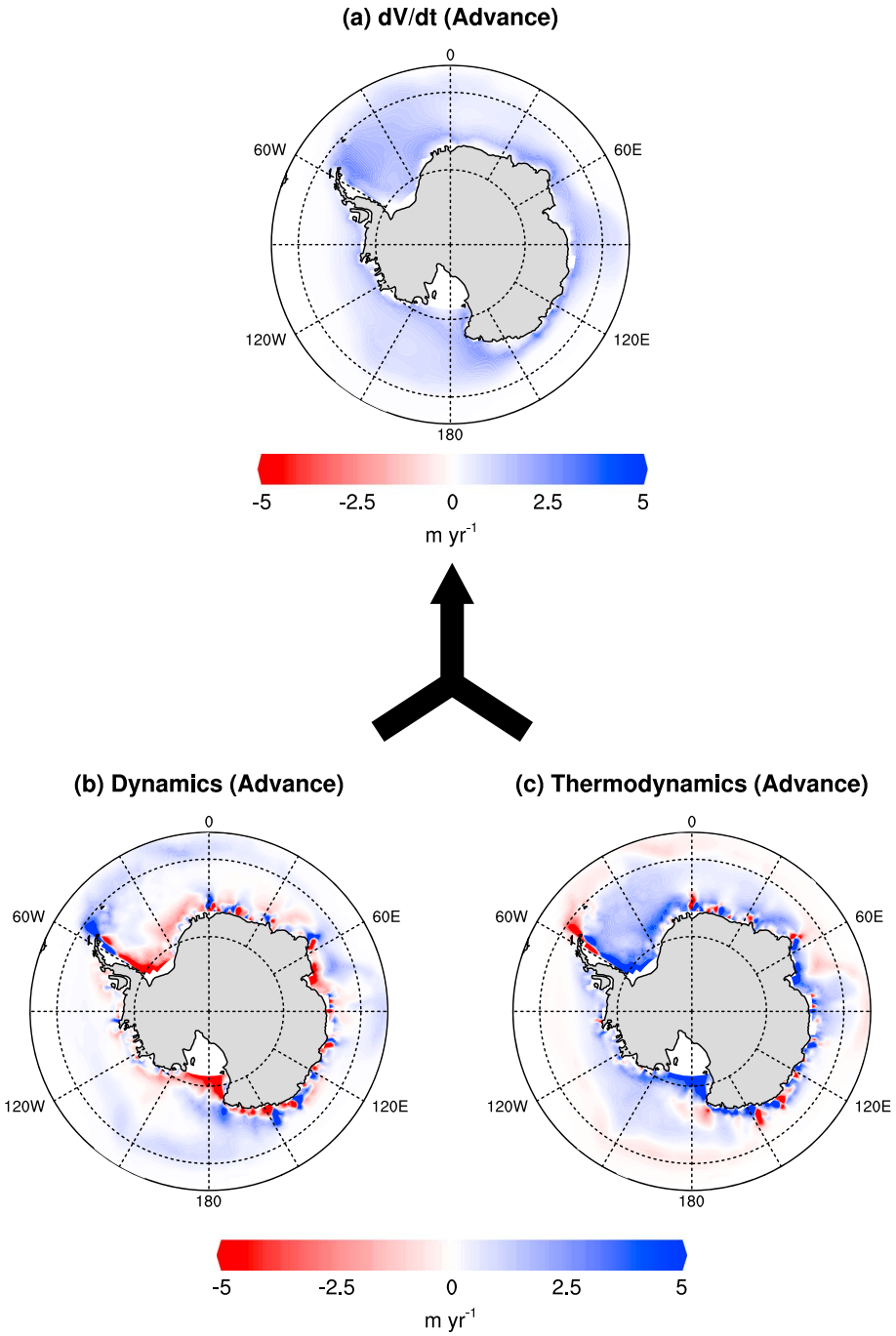

Figure 1. Example results showing Australian Community Climate and Earth System Simulator 1-0 (a) mean change in sea ice volume ($\partial V/\partial t$), where positive values indicate an increase in sea ice volume (blue shading), and the contribution to $\partial V/\partial t$ from (b) mean sea ice dynamics and (c) mean thermodynamics (freeze/melt) from the pre-industrial control experiment during the season of sea ice advance.

volume—suggesting divergent motion). The thermodynamic term (Figure 1c) is positive around the continental edge and in the central ice pack, positively contributing to the sea ice increase, and negative toward the ice edge where relatively warm temperatures melt sea ice. In this example, the autumn expansion of the central sea ice pack in ACCESS1-0 is dominated by the thermodynamic term in Figure 1c, while at the northernmost edge of the sea ice, dynamic processes become the major driver (Figure 1b). Both dynamic and thermodynamic processes play an important role in the coastal zone.

To quantify the relative magnitude of the dynamic and thermodynamic contributions to $\partial V/\partial t$, the three terms were integrated across six sea ice sectors and two sea ice zones. The sectors were defined as follows: the Ross Sea (163–200°E), the Amundsen Sea (200–250°E), the Bellingshausen Sea (250–293°E), the Weddell Sea (293–346°E), the King Hakon VII Sea (346–71°E), and East Antarctica (71–163°E), based on the regions of sea ice variability in Raphael and Hobbs (2014), except that the Amundsen and Bellingshausen Seas are separated in our analysis. The sea ice interior was defined as the area integrated from the coast up to 1° latitude south of the line of pre-industrial annual average maximum sea ice extent (i.e., the highest latitude at which sea ice concentration is at least 15% and sea ice thickness at least 20 cm). The sea ice edge was defined as the area integrated northward from 1° south of the line of maximum sea ice extent. This definition is similar to that of Kimura and Wakatsuchi (2011), who use a single grid point from the ice edge as the maximum extent of the interior of the sea ice pack. The percentage contribution of the dynamic term to $\partial V/\partial t$ was calculated for both the mean and trends (supporting information Tables S1 and S2) and is summarized as boxplots. The contributions of dynamic and thermodynamic processes to both mean and trends of $\partial V/\partial t$ are often much larger than $\partial V/\partial t$; in these cases, $\partial V/\partial t$ is the residual of the larger dynamic and thermodynamic terms, one of which nearly compensates entirely for the other, canceling each other out. This indicates that one of the terms acts to diminish $\partial V/\partial t$ rather than contributing positively toward its change.

We use monthly data since daily data were not available for all models at the time of the analysis; however, we repeated the calculations using the two models where daily data were available (ACCESS1-0 and IPSL-CM5A-LR) and include the results as supporting information (Figures S1–S2). For both models, the trends remained of the same sign, with minimal spatial differences between the monthly and daily data. The relative contributions of dynamic and thermodynamic processes were also consistent between the daily and monthly data. For the purposes of this analysis, we thus use monthly data for computational efficiency and to extend our analysis to the 10 model configurations.

After applying the sea ice volume budget calculation, the climatological means for C, $\partial V/\partial t$, dynamics, and the thermodynamic processes were calculated from the piControl and historical data. The piControl captured the nonevolving pre-industrial processes for each model. For the historical period, all models used here have at least three historical ensemble members, so the individual ensemble member trends of C, $\partial V/\partial t$, TRANSI, and the residual were calculated using an ordinary least squares regression over the period 1979–2005, encompassing the period from which satellite observations began until the end of the CMIP5 historical experiment. After calculating the trends, the ensembles were averaged into model ensemble mean trends. The mean state and trends were then averaged (weighted by the length of each month) into seasonal means for the seasons of sea ice advance (March to August) and retreat (October to February), based on Raphael and Hobbs (2014). Where plotted, trend significance averaged over the ensemble members for each model was estimated using a Student's t test.

3. Results

In this section, we first discuss differences between mean observed and simulated Antarctic sea ice, synthesizing model biases that may contribute to these differences. We then examine the mean simulated $\partial V/\partial t$ and the relative magnitude of the contributions to this change from dynamic and thermodynamic processes and consider the implications of mean sea ice flow regimes in the models. Following this, we investigate trends of simulated sea ice concentration, $\partial V/\partial t$, and the dynamic and thermodynamic contributions to sea ice volume change, identifying the dominant drivers of change in different sectors and seasons.

3.1. Mean Sea Ice in CMIP5 Models

The observed mean and trends of Antarctic sea ice concentration are shown for comparison with the CMIP5 models examined in the following section. In the observed mean state during advance (Figure 2a) and retreat (Figure 2b), high sea ice concentration in the Ross and Weddell Seas, which are known to be major sea ice production zones, can be seen. Trends in sea ice concentration during advance (Figure 2c) and retreat (Figure 2d) show a spatially heterogeneous pattern that is mostly similar across the two seasons in most regions, with a large increase in the Ross, King Hakon VII, and eastern Weddell Seas and a decrease of similar magnitude in the Amundsen, Bellingshausen, and western Weddell Seas.

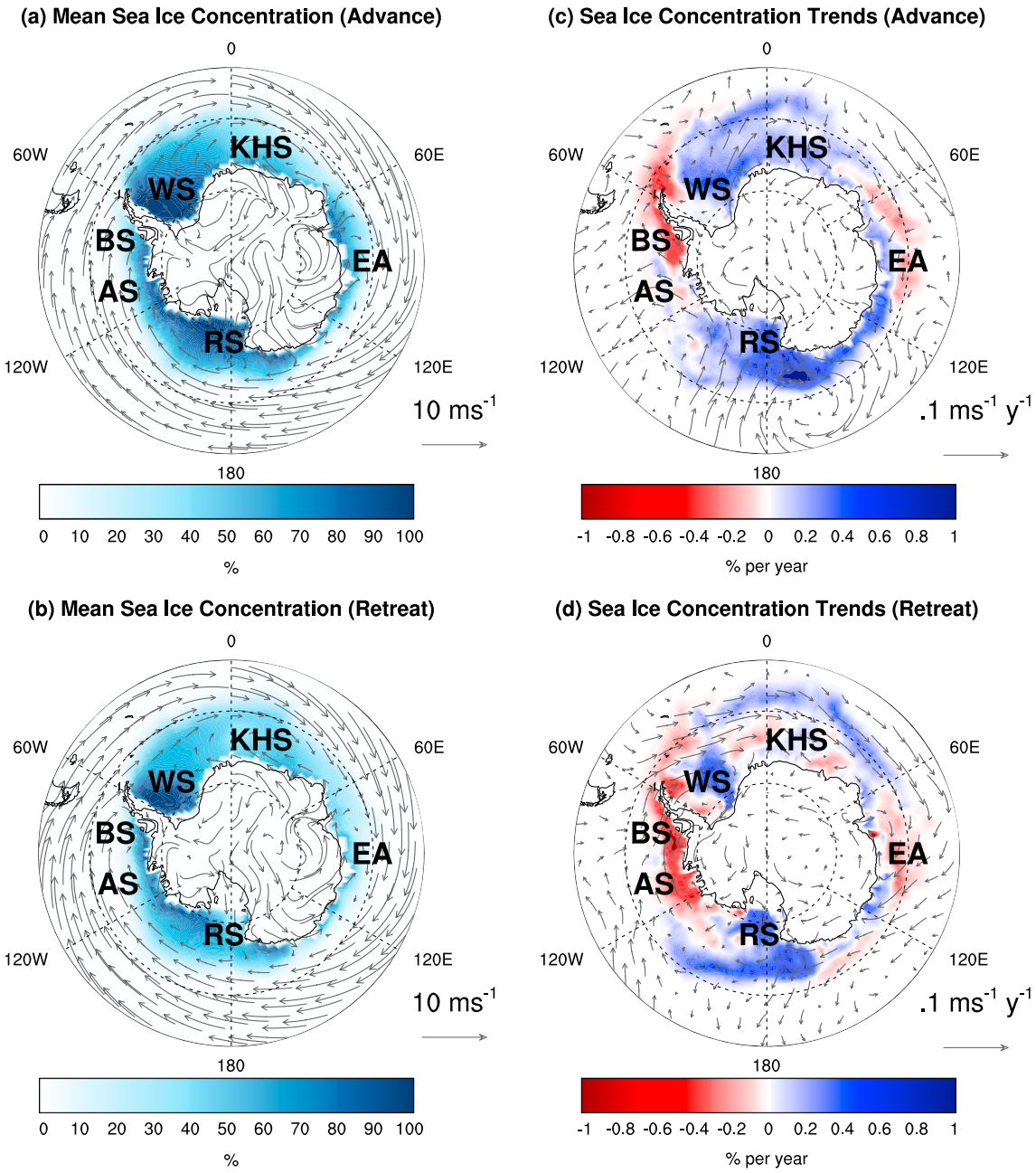

Figure 2. National Snow and Ice Data Center sea ice concentration and ERA-Interim 10-m winds (a) mean during sea ice advance; (b) mean during sea ice retreat; (c) 1979–2005 trends during sea ice advance; and (d) 1979–2005 trends during sea ice retreat, in the King Hakon VII Sea (KHS), East Antarctica (EA), Ross Sea (RS), Amundsen Sea (AS), Bellingshausen Sea (BS), and Weddell Sea (WS).

The 10 model formulations examined in this study produce different magnitudes of mean sea ice concentration and surface winds and encompass a range of biases compared to the observations (Figure 3). Here we compare the model biases in mean sea ice by subtracting the observed mean (Figures 2a and 2b) from each model mean.

The ACCESS model was built with the intention of producing a global coupled climate model with a Southern Hemisphere focus (Puri, 2012). The two versions, ACCESS1-0 and ACCESS1-3, use different land surface and cloud physics schemes. Both models produce a cold near-surface air temperature bias in the high southern latitudes, particularly over coastal sea ice. The cloud scheme used by ACCESS1-3 produces more clouds than

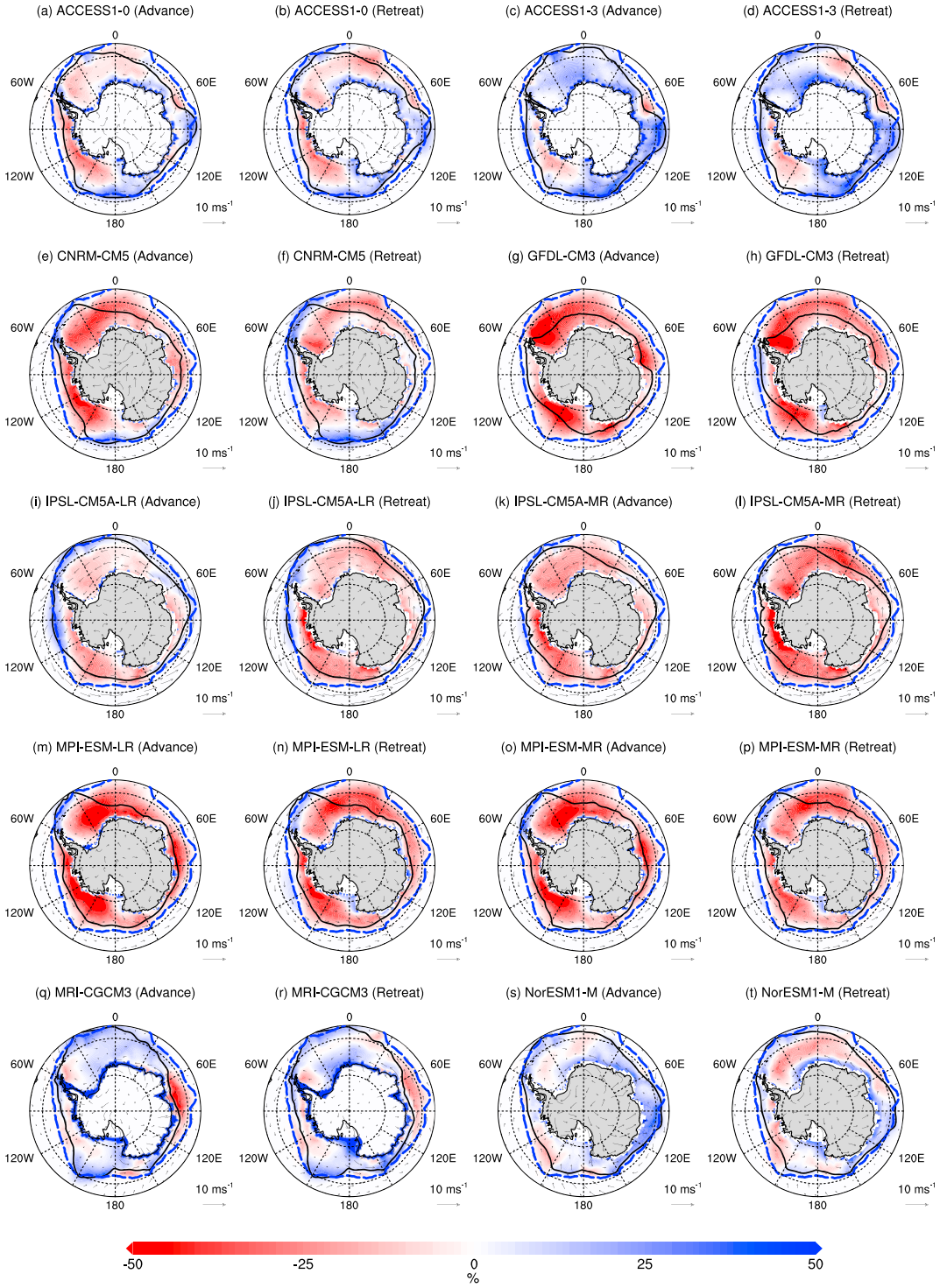

Figure 3. Mean sea ice concentration bias (National Snow and Ice Data Center observations; shading) and mean surface wind bias (ERA-Interim reanalysis; arrows), with the 15% sea ice concentration isoline depicting the winter maximum ice edge from the preindustrial control experiment during the seasons of sea ice advance and retreat in (a, b) ACCESS1-0, (c, d) ACCESS1-3, (e, f) CNRM-CM5, (g, h) GFDL-CM3, (i, j) IPSL-CM5A-LR, (k, l) IPSL-CM5A-MR, (m, n) MPI-ESM-LR, (o, p) MPI-ESM-MR, (q, r) MRI-CGCM3, and (s, t) NorESM1-M. Blue shading shows where the model simulation overestimates sea ice concentration. ACCESS = Australian Community Climate and Earth System Simulator; CNRM-CM5 = Centre National de Recherches Météorologiques Climate Model version 5; GFDL-CM3 = Geophysical Fluid Dynamics Laboratory Climate Model version 3; IPSL-CM5A-LR = Community Climate System Model and Institut Pierre Simon Laplace Low-Resolution model; IPSL-CM5A-MR = Community Climate System Model and Institut Pierre Simon Laplace Middle-Resolution model; MPI-ESM-LR = Max Planck Institute Earth System Low-Resolution model; MPI-ESM-MR = Max Planck Institute Earth System Mixed-Resolution model; MRI-CGCM3 = Meteorological Research Institute coupled global climate model; NorESM1-M = Norwegian Climate Center's Earth System Model.

the scheme used by ACCESS1-0, which reduces the high-latitude cold bias in ACCESS1-3. However, due to a higher albedo in ACCESS1-3 than in ACCESS1-0, mean surface air temperatures in ACCESS1-3 are still up to 1.66 °C colder than ACCESS1-0 over the Southern Ocean south of 60°S (Bi et al., 2013; Uotila et al., 2013). Compared with satellite observations (Figures 2a and 2b), ACCESS1-0 largely underestimates sea ice concentration during advance and retreat (Figures 3a and 3b), while ACCESS1-3 overestimates sea ice concentration in most regions during both advance and retreat (Figures 3c and 3d), and particularly in the Weddell Sea. The higher albedo in ACCESS1-3 is known to produce overly thick sea ice from the eastern Weddell Sea around East Antarctica (Bi et al., 2013; Uotila et al., 2013). Both ACCESS1-0 and ACCESS1-3 generally produce Antarctic sea ice metrics that are reasonably close to satellite observations in comparison with other models in the CMIP5 suite. However, sea ice variability in ACCESS1-0 is too high, and both models overestimate winter sea ice extent, while ACCESS1-0 underestimates and ACCESS1-3 overestimates summer extent (Uotila et al., 2013).

The Centre National de Recherches Météorologiques (CNRM)-Groupe d'études de l'Atmosphère Météorologique and the Centre Européen de Recherche et de Formation Avancée joint coupled climate model CNRM-CM5 has a low mean state of sea ice concentration and extent (Figures 3e and 3f) compared with satellite observations (Figures 2a and 2b). The model is known to generally underestimate sea ice, particularly extent, with too little summer sea ice (Turner et al., 2013). A warm bias in the upper-ocean layers enhances sea ice melt during sea ice retreat and suppresses sea ice production during the following growth season (Voldoire et al., 2013). Overestimated sea level pressure over the Southern Ocean also results in underestimated surface wind stress, which is likely to produce a low mean northward sea ice transport.

The National Oceanic and Atmospheric Administration's Geophysical Fluid Dynamics Laboratory Climate Model version 3 (GFDL-CM3) produces very low sea ice concentration and extent during both sea ice advance and retreat seasons (Figures 3g and 3h). The model is known to underestimate mean sea ice extent and area, with summer sea ice disappearing almost entirely due to a warm ocean bias (Griffies et al., 2011).

The IPSL-CM5 model has two different horizontal resolutions in the atmosphere, with grid spacings of 3.75° latitude × 1.875° longitude in the low-resolution model (IPSL-CM5A-LR) and of 2.5° latitude × 1.25° longitude in the medium-resolution model (IPSL-CM5A-MR; Dufresne et al., 2013). The two models both show a low mean state of sea ice concentration and extent, which is more pronounced in IPSL-CM5A-MR (Figures 3k and 3l) than in IPSL-CM5A-LR (Figures 3i and 3j). There is little difference between the models in terms of cloud effects or global temperature bias, with both producing a warm surface temperature bias in the high latitudes that leads to low mean state of annual sea ice extent and volume (Dufresne et al., 2013).

The two versions of the MPI-ESM differ in their vertical and horizontal resolution. The low-resolution model (MPI-ESM-LR) and the mixed-resolution model (MPI-ESM-MR) differ in their vertical atmosphere levels, with 47 levels in MPI-ESM-LR compared with 95 in MPI-ESM-MR. The grid resolution and mapping also differ, from 1.5° and two grid poles in MPI-ESM-LR to 0.4° on a tripolar grid in MPI-ESM-MR. Both versions have a low mean state of Antarctic sea ice throughout the year (Figures 3m–3p) and are known to be biased warm and salty in the intermediate and deep ocean, with overestimated downwelling shortwave radiation into the Southern Ocean causing a warm surface layer and low mean sea ice (Jungclaus et al., 2013). The warm bias in the ocean has implications for vertical heat entrainment by brine rejection during sea ice formation (Goosse et al., 1997; Martinson, 1990). Both models are thought to overestimate convection in the open ocean while underestimating dense shelf water formation, as well as producing deep convection and vertical heat transport in the Weddell and Ross gyres, which implies biases in the freeze-thaw-transport cycle of sea ice (Jungclaus et al., 2013).

The mean state of sea ice in the Meteorological Research Institute coupled global climate model (MRI-CGCM3) is close to observations, but it overestimates sea ice extent during both advance and retreat (Figures 3q and 3r), like the ACCESS models. Maximum sea ice extent in the Weddell Sea in particular exceeds that which is observed in the satellite record. MRI-CGCM3 produces an overly deep Amundsen Sea Low for most of the year, which results in overly extensive sea ice in the Ross Sea and low extent in the Amundsen and Bellingshausen Seas (Hosking et al., 2013). MRI-CGCM3 is also known to underestimate cloud forcing, which leads to a surface warm bias over the Southern Ocean, while high precipitation driving an overestimated global water cycle enhances the freshwater flux at the ocean surface in the high latitudes (Yukimoto et al., 2012). The high freshwater flux may lead to excessive stratification of the ocean mixed

layer around Antarctica and thus reduced ocean heat ventilation (Sallée et al., 2013), permitting extensive mean sea ice despite the warm surface temperatures.

The Norwegian Climate Center's Earth System Model (NorESM1-M) has one of the better representations of the annual Antarctic sea ice extent cycle among CMIP5 models, given that many models underestimate mean sea ice extent (Turner et al., 2013). However, the model still overestimates sea ice concentration and extent during both advance and retreat (Figures 3s and 3t). NorESM1-M overestimates sea ice thickness in regions such as the Weddell Sea, maintaining too much sea ice throughout summer (Bentsen et al., 2012), and has one of the largest mean sea ice states of the CMIP5 models (Turner et al., 2013).

The model sea ice concentration biases in Figure 3 fall within −50% to +50% of mean observed sea ice concentration, suggesting that the largest underestimation is approximately half the observed concentration at the most, while the overestimation is up to 50% more than observed. In most regions, however, the modeled sea ice bias is much smaller than these maximum values. The models that most strongly overestimate mean Antarctic sea ice relative to satellite observations are ACCESS1-0, ACCESS1-3, MRI-CGCM3, and NorESM1-M, though all of the models somewhat overestimate sea ice concentration in at least one location around the continent in at least one season, particularly toward the ice edge. The majority of models (all except ACCESS1-3 and MRI-CGCM3) underestimate mean sea ice concentration around the continent; some, such as GFDL-CM3, MPI-ESM-LR, and MPI-ESM-MR, have quite large underestimations, particularly during the season of sea ice advance. The mean state of sea ice strongly influences sea ice trends in CMIP5 models; for example, models with substantially lower mean sea ice concentration and extent than observed will not produce negative trends of sea ice which reflect observed spatial patterns (Turner et al., 2013).

3.2. Mean Sea Ice Volume Budgets in CMIP5 Models

Mean sea ice volume change ($\partial V/\partial t$; Figure 4) highlights the different behavior of sea ice between the models. The seasonal sea ice increase and decrease in MRI-CGCM3 (Figures 4q and 4r) is the most spatially extensive, reaching further north than any other model. Models with greater sea ice concentration, such as ACCESS1-0, ACCESS1-3, MRI-CGCM3, and NorESM1-M (Figures 41–4d and 4q–4t), have a high-magnitude seasonal cycle with strong $\partial V/\partial t$ in regions away from the coast as well as around the coastline. This has important implications for ocean convection, as strong seasonal sea ice production away from the coast is associated with open ocean deep convection, rather than bottom water produced from dense shelf water as is observed (Heuzé et al., 2013). By comparison, the annual sea ice cycle away from the coast in models such as GFDL-CM3 (Figures 4g and 4h), MPI-ESM-LR (Figures 4m and 4n), and MPI-ESM-MR (Figures 4o and 4p) is much smaller; these models are among those that most underestimate mean sea ice compared with observations.

In more than half of the models (ACCESS1-0, ACCESS1-3, IPSL-CM5A-LR, IPSL-CM5A-MR, MPI-ESM-LR, MPI-ESM-MR, and NorESM1-M), $\partial V/\partial t$ is particularly strong at the tip of the Antarctic Peninsula and extends across the north of the Weddell Sea (Figures 4a–4d, 4i–4p, and 4s and 4t). This is the region with the largest observed net sea ice production at the circumpolar sea ice edge (Kimura & Wakatsuchi, 2011). The majority of the models also have strong $\partial V/\partial t$ around the coast of East Antarctica (particularly ACCESS1-0, ACCESS1-3, CNRM-CM5, MPI-ESM-LR, MPI-ESM-MR, MRI-CGCM3, and NorESM1-M; Figures 4a–4f and 4m–4t), which is also in agreement with the high observed ice production in this region (Kimura & Wakatsuchi, 2011).

The relative magnitudes of the dynamic contribution to overall $\partial V/\partial t$ in the sea ice interior and at the ice edge of each sector are summarized in multimodel boxplots in Figure 5. The boxplots show the models are largely in agreement in the mean, though with a large intermodel spread in East Antarctica at the ice edge in both seasons. During advance, ice gain in the ice interior is dominated by thermodynamic processes, while the ice edge is generally dominated by dynamic processes (Figure 5a). During retreat, thermodynamics dominate in the interior and at the ice edge (Figure 5b). Individual model contributions are shown in Table S1. In some models and sectors, the sign of the nondominant term is negative, indicating that the effect of the term acts to oppose the total change in sea ice. In these cases, the magnitude of the dominant process is large enough to compensate for the negative term. For example, in the interior sea ice zone of the Ross Sea in ACCESS1-0 during advance, though the overall sea ice change is positive, negative dynamics oppose this overall change (contributing −17.6% to $\partial V/\partial t$) by transporting the ice away from the interior. The thermodynamic term (contributing 117.6% of $\partial V/\partial t$) then compensates for the transported sea ice, as the open ocean surface is

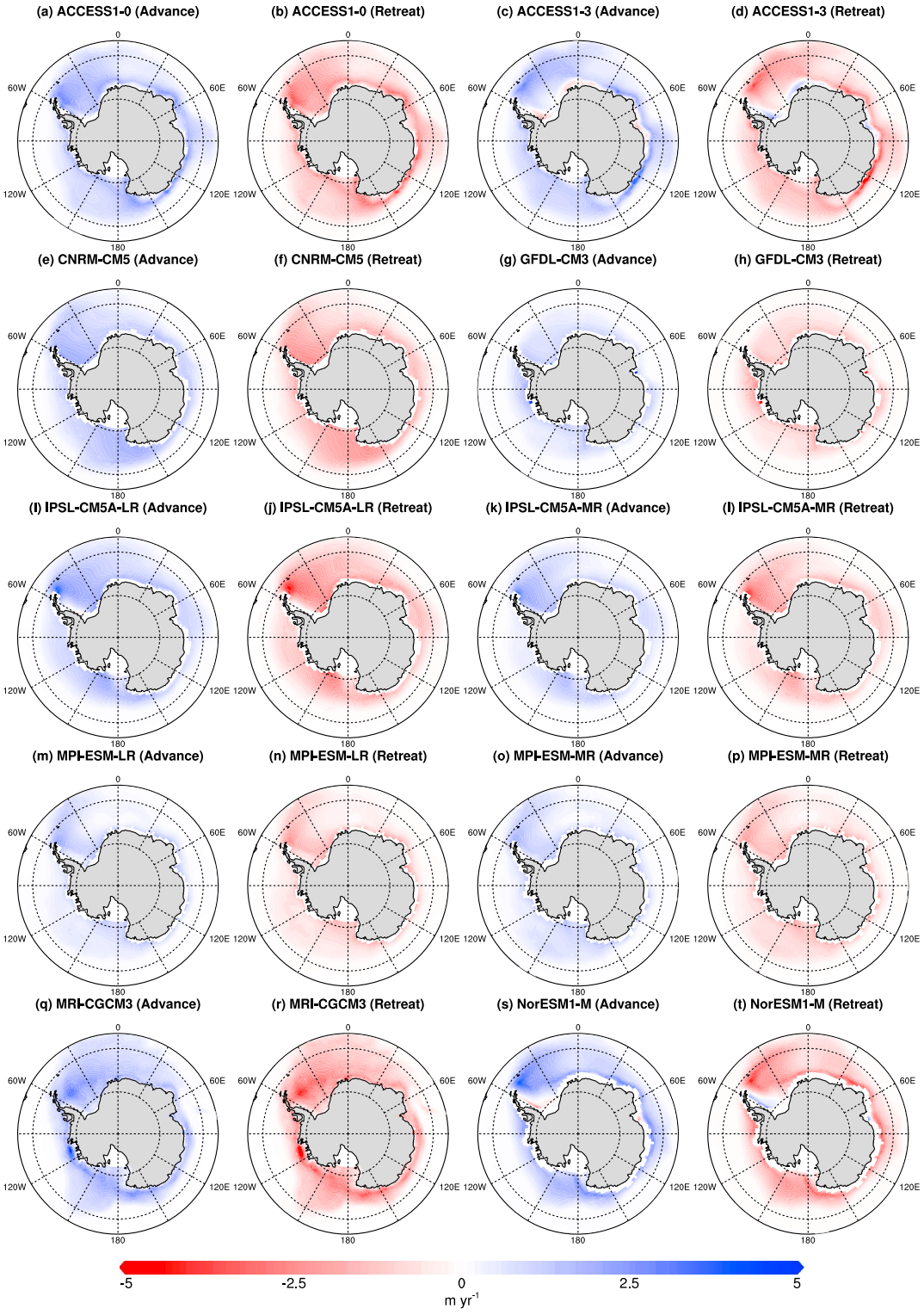

Figure 4. Mean $\partial V/\partial t$ from the preindustrial control experiment during the seasons of sea ice advance and retreat in (a, b) ACCESS1-0, (c, d) ACCESS1-3, (e, f) CNRM-CM5, (g, h) GFDL-CM3, (i, j) IPSL-CM5A-LR, (k, l) IPSL-CM5A-MR, (m, n) MPI-ESM-LR, (o, p) MPI-ESM-MR, (q, r) MRI-CGCM3, (s, t) and NorESM1-M. ACCESS = Australian Community Climate and Earth System Simulator; CNRM-CM5 = Centre National de Recherches Météorologiques Climate Model version 5; GFDL-CM3 = Geophysical Fluid Dynamics Laboratory Climate Model version 3; IPSL-CM5A-LR = Community Climate System Model and Institut Pierre Simon Laplace Low-Resolution model; IPSL-CM5A-MR = Community Climate System Model and Institut Pierre Simon Laplace Middle-Resolution model; MPI-ESM-LR = Max Planck Institute Earth System Low-Resolution model; MPI-ESM-MR = Max Planck Institute Earth System Mixed-Resolution model; MRI-CGCM3 = Meteorological Research Institute coupled global climate model; NorESM1-M = Norwegian Climate Center's Earth System Model.

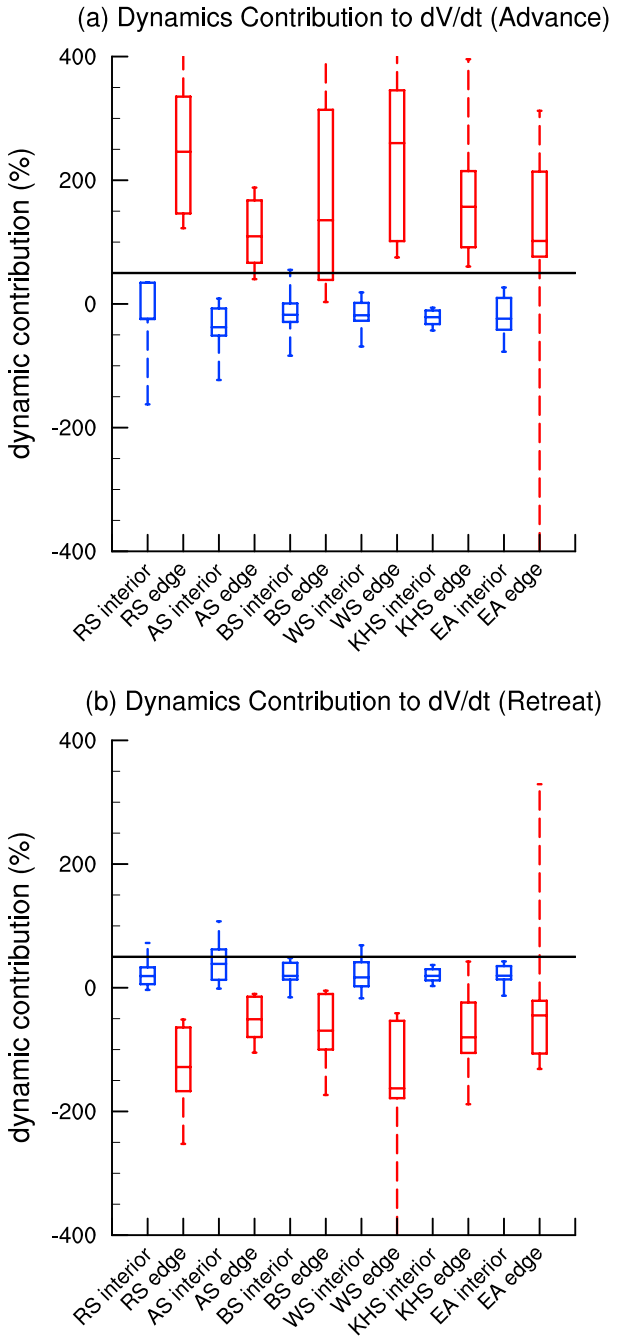

Figure 5. Relative dynamic contribution to mean $\partial V/\partial t$ (as a percentage of total $\partial V/\partial t$) during advance (a) and retreat (b) in the Ross Sea (RS), Amundsen Sea (AS), Bellingshausen Sea (BS), Weddell Sea (WS), King Hakon VII Sea (KHS), and East Antarctic (EA) sectors at the sea ice interior (blue) and edge (red). Boxes show the 20–80% quartile range. Black line indicates 50% positive contribution to $\partial V/\partial t$; median values above this line show sectors and seasons where dynamic processes dominate $\partial V/\partial t$, and values below show where thermodynamic processes dominate. Negative values show where dynamic processes oppose the sign of the total $\partial V/\partial t$ term; positive values show where they contribute positively toward $\partial V/\partial t$.

exposed to cold surface temperatures that drive sea ice growth in the interior sea ice zone. This compensation is more prominent at the ice edge during both seasons, as most models show an opposite sign in the thermodynamic and dynamic contribution. During retreat in the interior sea ice zone, however, the dynamic and thermodynamic contributions generally agree in sign, indicating that both processes positively contribute to seasonal ice melt.

All models examined here show positive contribution from sea ice dynamics at the ice edge during both seasons, particularly to the north of the Weddell Sea, western Ross Sea, and East Antarctic region (Figure 6). Wind-driven sea ice motion drives the ice northward where relatively warm temperatures prevent ice formation and induce melting (Massom, 1992), as shown by the negative thermodynamic contribution at the ice edge in both seasons (Figure 7). At the coast, northward sea ice motion is evident in all models; however, there are areas of positive coastal sea ice dynamics in some models, particularly in the major ice production zones of the Weddell and Ross Seas. Coastal convergence could be due to easterly winds constraining ice transport, or to overestimated sea ice velocities as has been previously found in the ACCESS models (Uotila et al., 2014).

Thermodynamic processes generally dominate the sea ice retreat season both in the ice interior and at the ice edge (Figure 5b). Models such as GFDL-CM3, MPI-ESM-MR, and MRI-CGCM3 (Figures 7g and 7h and 7o–7r) show only melt, while the remaining models retain some positive thermodynamic values during retreat. In 6 of the 10 models, there are substantial slivers of the coastline where the thermodynamic contribution reverses sign during advance, potentially indicating the presence of coastal polynyas or anomalous ice flow due to the coastal topography. The sign reversal is particularly noticeable around the Weddell Sea and East Antarctica coasts in ACCESS1-3 (Figures 6c and 6d), along the eastern coast of the West Antarctic Peninsula in IPSL-CM5A-LR (Figures 6i and 6j) and NorESM1-M (Figures 6s and 6t), and along the coast of East Antarctica west of the Ross Sea in MPI-ESM-LR (Figures 6m and 6n).

Overall, the contribution of sea ice dynamics to net $\partial V/\partial t$ is lower in GFDL-CM3, MPI-ESM-MR, and MRI-CGCM3 (Figures 6g and 6h and 6o–6r) than in other models, suggesting that in these models, thermodynamic processes may play a stronger role in $\partial V/\partial t$. By comparison, ACCESS1-0, ACCESS1-3, and NorESM1-M generally produce high-magnitude mean sea ice concentration and extent as well as high-magnitude dynamic and thermodynamic terms compared with other models. It is interesting to note that ACCESS1-0, ACCESS1-3, and NorESM1-M all use the Los Alamos Community Ice CodE (CICE) as their sea ice component (Table 1), and all produce a similar pattern and magnitudes of mean sea ice concentration and dynamics. The higher-magnitude sea ice dynamics in the models using CICE may simply reflect the high-magnitude mean concentration and extent; however, it could also indicate a sensitivity of the CICE component to aspects such as sea ice drift speed or turning angle, which has been shown in an ACCESS study to influence the contribution of dynamics to changes in sea ice concentration (Uotila et al., 2014).

3.2.1. Mean Sea Ice Transport in CMIP5 Models

As discussed above, all 10 models show sea ice dynamics (Figure 6) to be an important determinant of mean $\partial V/\partial t$. However, as well as strong differences in the magnitude of sea ice dynamics between the models, the vector quantity depicting sea ice mass transport shows markedly

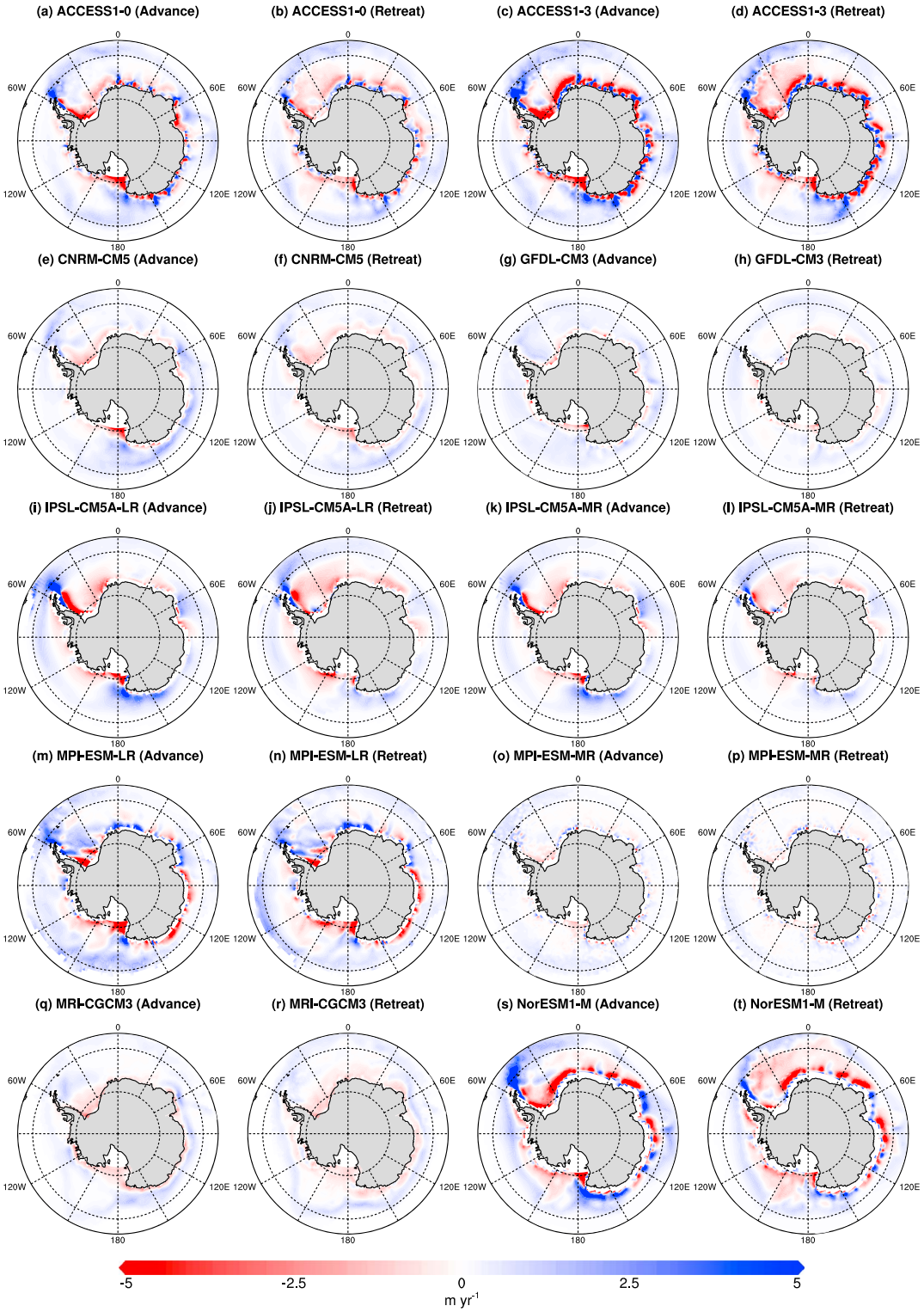

Figure 6. Mean dynamic contribution to $\partial V/\partial t$ from the preindustrial control experiment during the seasons of sea ice advance and retreat in (a, b) ACCESS1-0, (c, d) ACCESS1-3, (e, f) CNRM-CM5, (g, h) GFDL-CM3, (i, j) IPSL-CM5A-LR, (k, l) IPSL-CM5A-MR, (m, n) MPI-ESM-LR, (o, p) MPI-ESM-MR, (q, r) MRI-CGCM3, and (s, t) NorESM1-M. ACCESS = Australian Community Climate and Earth System Simulator; CNRM-CM5 = Centre National de Recherches Météorologiques Climate Model version 5; GFDL-CM3 = Geophysical Fluid Dynamics Laboratory Climate Model version 3; IPSL-CM5A-LR = Community Climate System Model and Institut Pierre Simon Laplace Low-Resolution model; IPSL-CM5A-MR = Community Climate System Model and Institut Pierre Simon Laplace Middle-Resolution model; MPI-ESM-LR = Max Planck Institute Earth System Low-Resolution model; MPI-ESM-MR = Max Planck Institute Earth System Mixed-Resolution model; MRI-CGCM3 = Meteorological Research Institute coupled global climate model; NorESM1-M = Norwegian Climate Center's Earth System Model.

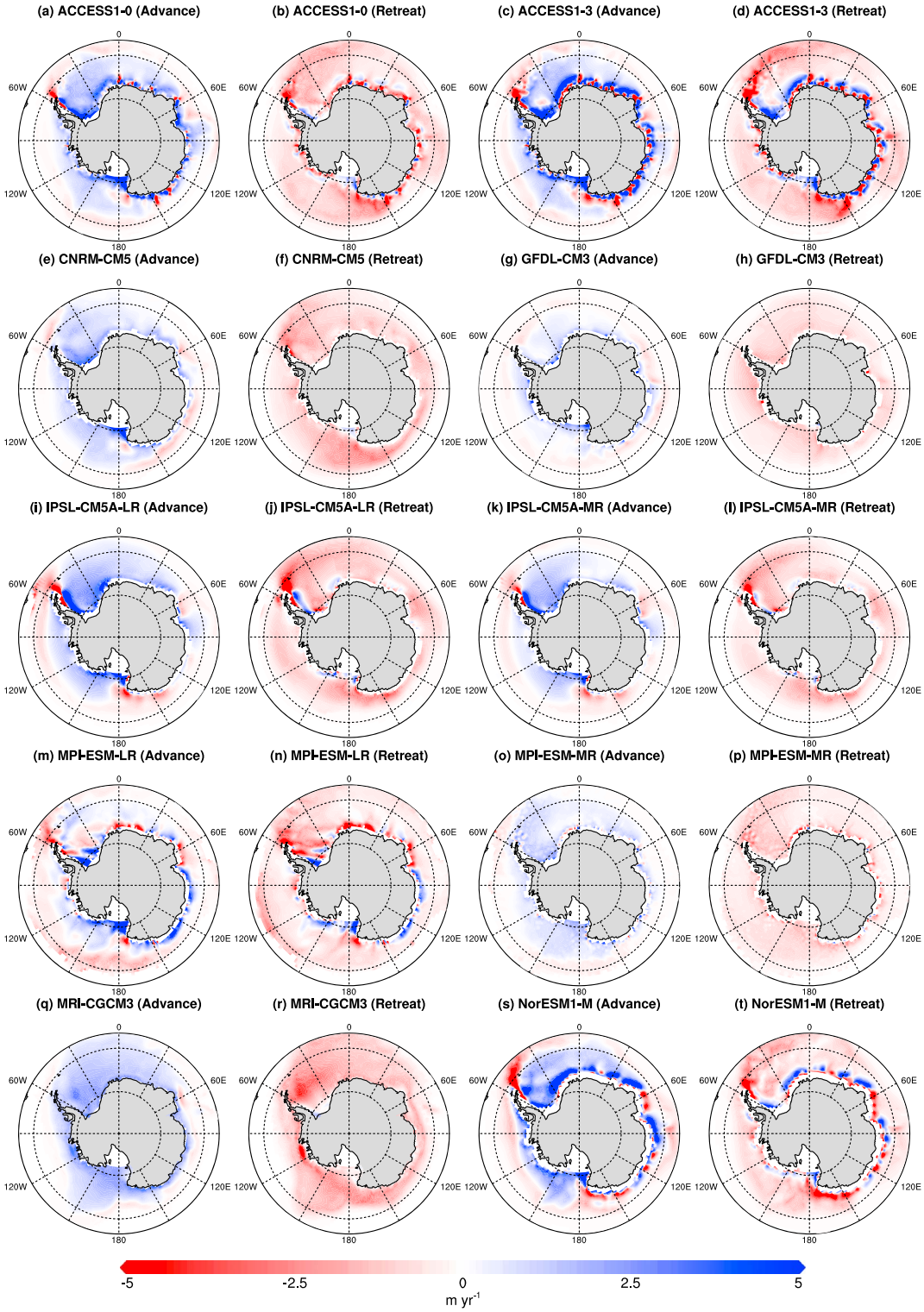

Figure 7. As in Figure 6 but showing mean thermodynamic (freeze/melt) contribution to $\partial V/\partial t$, from the preindustrial control experiment during the seasons of sea ice advance and retreat in (a, b) ACCESS1-0, (c, d) ACCESS1-3, (e, f) CNRM-CM5, (g, h) GFDL-CM3, (i, j) IPSL-CM5A-LR, (k, l) IPSL-CM5A-MR, (m, n) MPI-ESM-LR, (o, p) MPI-ESM-MR, (q, r) MRI-CGCM3, and (s, t) NorESM1-M. ACCESS = Australian Community Climate and Earth System Simulator; CNRM-CM5 = Centre National de Recherches Météorologiques Climate Model version 5; GFDL-CM3 = Geophysical Fluid Dynamics Laboratory Climate Model version 3; IPSL-CM5A-LR = Community Climate System Model and Institut Pierre Simon Laplace Low-Resolution model; IPSL-CM5A-MR = Community Climate System Model and Institut Pierre Simon Laplace Middle-Resolution model; MPI-ESM-LR = Max Planck Institute Earth System Low-Resolution model; MPI-ESM-MR = Max Planck Institute Earth System Mixed-Resolution model; MRI-CGCM3 = Meteorological Research Institute coupled global climate model; NorESM1-M = Norwegian Climate Center's Earth System Model.

different behavior in flow regimes between the models (Figure 8). There is a general tendency among the models to transport large amounts of sea ice around the Ross and Weddell gyres, with a cyclonic pattern in East Antarctica as well, consistent with observed sea ice motion (Holland & Kwok, 2012). The magnitude of sea ice transport, particularly around the coast in ACCESS1-0, ACCESS1-3, IPSL-CM5A-LR, and NorESM1-M, is noticeably larger than in other models. A large amount of sea ice tends to move around the coastline in ACCESS1-0, ACCESS1-3, GFDL-CM3, IPSL-CM5A-LR, IPSL-CM5A-MR, and NorESM1-M before turning northward, whereas in CNRM-CM5, MPI-ESM-LR, MPI-ESM-MR, and particularly in MRI-CGCM3, the tendency appears to be for ice to move northward rather than following the coastal currents.

As discussed above, the CICE models (ACCESS1-0, ACCESS1-3, and NorESM1-M) have higher-magnitude mass transport than the other models, associated with large sea ice volume biases. However, MRI-CGCM3, which also has a large positive bias in mean sea ice, produces a relatively small magnitude of sea ice mass transport that is predominantly northward flowing rather than vortical as in the ACCESS models and NorESM1-M. The other models all have smaller sea ice mass transport, associated with negative mean sea ice biases, as discussed above. Biases in the speed and direction of sea ice velocity, particularly at the ice edge, substantially limit model capability to accurately reproduce rates of sea ice advance and retreat and should therefore be a key focus for future model improvements (Lecomte et al., 2016).

3.3. Sea Ice Volume Budget Trends in CMIP5 Models

Given that the 10 models used in this study produce such different mean sea ice concentrations (Figure 3) and mass transports (Figure 8), we now consider the level to which dynamic or thermodynamic processes dominate sea ice change in the historical simulations. We note that simulated trends shown here are ensemble means for each model, so have less noise than observed trends which present a single realization of the climate. Trends in both observed (Figures 2c and 2d) and simulated sea ice and wind (in all models except CNRM-CM5) are spatially heterogeneous (Figure 9). However, the models show largely decreasing trends, especially around East Antarctica. None of the models capture the observed increase in the western Ross Sea (Figures 2c and 2d). GFDL-CM3, MPI-ESM-LR, and MPI-ESM-MR (Figures 9g and 9h, and 9m–9p) show increasing sea ice in parts of the Ross, Amundsen, and Bellingshausen Seas despite local poleward wind trends during advance in GFDL-CM3 and during retreat for both MPI models. As discussed above, GFDL-CM3, MPI-ESM-LR, and MPI-ESM-MR have among the lowest mean sea ice concentration and extent compared with observations (Figures 3g and 3h and 3m–3p), whereas models with more realistic sea ice concentration and extent (ACCESS1-0, ACCESS1-3, MRI-CGCM3, and NorESM1-M) produce smaller, more spatially variable and lower-magnitude sea ice increases in the Ross, Weddell, and King Hakon VII Seas, that is, where there are observed increases. The sea ice trends occur alongside increasing meridional wind trends in most models, particularly around West Antarctica where cyclonic flow is generally strengthening. All 10 models produce strengthening westerly winds around East Antarctica during retreat, which in ACCESS1-3, GFDL-CM3, IPSL-CM5A-LR, IPSL-CM5A-MR, and MPI-ESM-LR is part of a Southern Annular Mode-like zonal wind intensification. In more than half the models, the intensified westerly winds coincide with decreasing sea ice around East Antarctica. CNRM-CM5 is the only model to produce entirely decreasing sea ice concentration trends around Antarctica, which are strongest during retreat and in the Weddell Sea (Figures 9e and 9f).

The spatial heterogeneity of modeled sea ice trends is also apparent in trends in $\partial V/\partial t$ (Figure 10), showing trends in the temporal derivative of sea ice volume. Trends in $\partial V/\partial t$ show opposing signs between advance and retreat, reflecting the change in sea ice volume between the seasons. For example, trends of $\partial V/\partial t$ in CNRM-CM5 are negative during advance, indicating a reduction in autumn sea ice production, while positive trends during retreat indicate reduced ice melt (Figures 10e and 10f). Other than CNRM-CM5, the models have spatially-heterogeneous trends in $\partial V/\partial t$. For example, IPSL-CM5A-LR has reduced spring ice melt in the Weddell and King Hakon Seas (Figure 10j), even though there is a negative sea ice concentration trend in the same region (Figure 9j); presumably, this occurs because there is less ice to melt following the reduced ice growth season (Figures 9i and 10i).

Boxplots show the relative magnitudes of the dynamic contribution to $\partial V/\partial t$ trends (Figure 11). (Values for the integrated contributions of dynamic and thermodynamic processes for individual models are shown in Table S2. Note that extremely high percentage contributions occur where the total $\partial V/\partial t$ is low and the thermodynamic and dynamic terms compensate each other; these values are not represented in Figure 11.) During advance (Figure 11a), the model trends tend to be dominated by thermodynamics in the ice pack

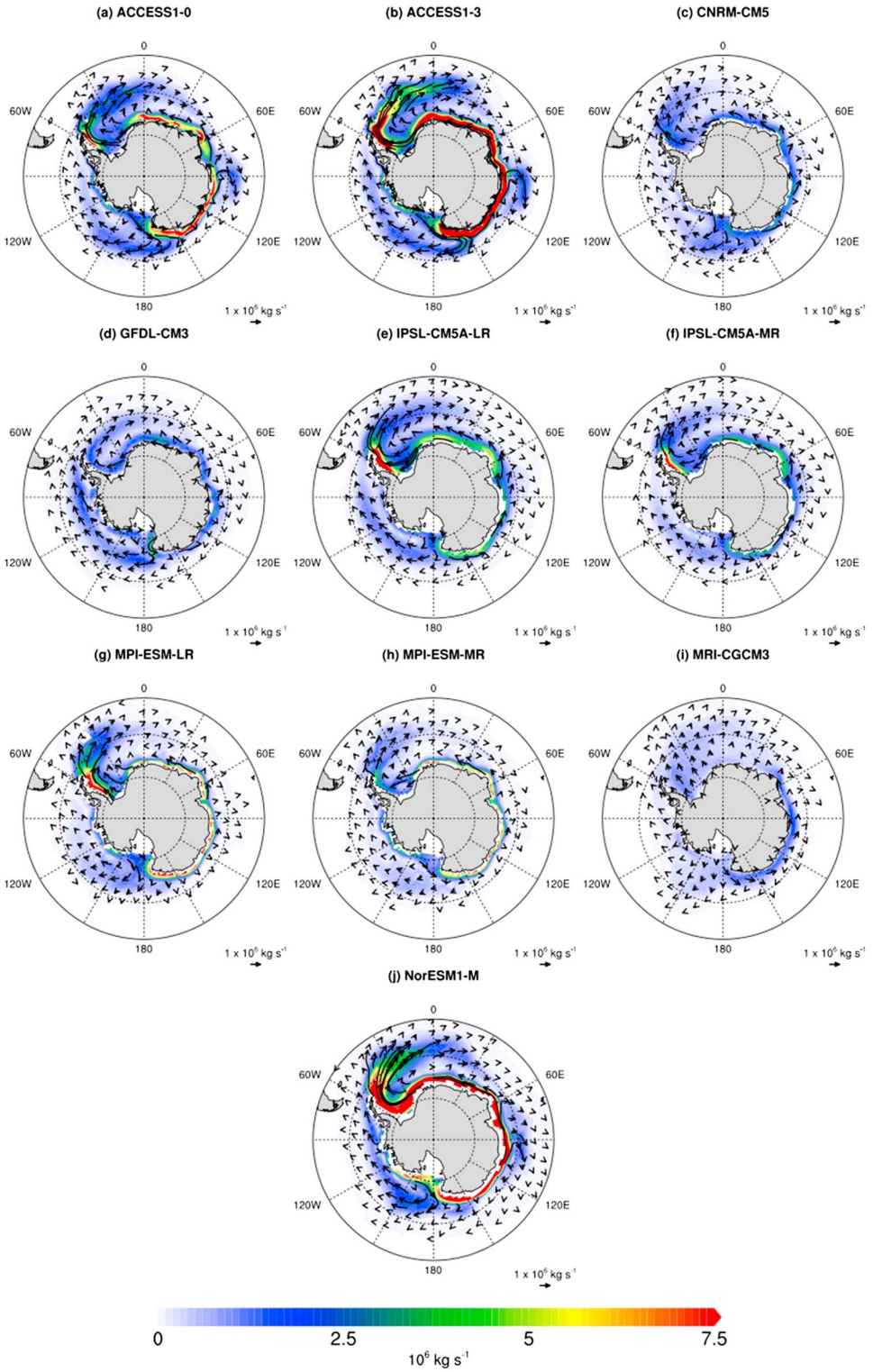

Figure 8. Mean annual sea ice mass transport (total mass transport shown by shading; direction of mass transport shown by arrows) in the Southern Ocean from the preindustrial control experiment in (a) ACCESS1-0, (b) ACCESS1-3, (c) CNRM-CM5, (d) GFDL-CM3, (e) IPSL-CM5A-LR, (f) IPSL-CM5A-MR, (g) MPI-ESM-LR, (h) MPI-ESM-MR, (i) MRI-CGCM3, and (j) NorESM1-M. ACCESS = Australian Community Climate and Earth System Simulator; CNRM-CM5 = Centre National de Recherches Météorologiques Climate Model version 5; GFDL-CM3 = Geophysical Fluid Dynamics Laboratory Climate Model version 3; IPSL-CM5A-LR = Community Climate System Model and Institut Pierre Simon Laplace Low-Resolution model; IPSL-CM5A-MR = Community Climate System Model and Institut Pierre Simon Laplace Middle-Resolution model; MPI-ESM-LR = Max Planck Institute Earth System Low-Resolution model; MPI-ESM-MR = Max Planck Institute Earth System Mixed-Resolution model; MRI-CGCM3 = Meteorological Research Institute coupled global climate model; NorESM1-M = Norwegian Climate Center's Earth System Model.

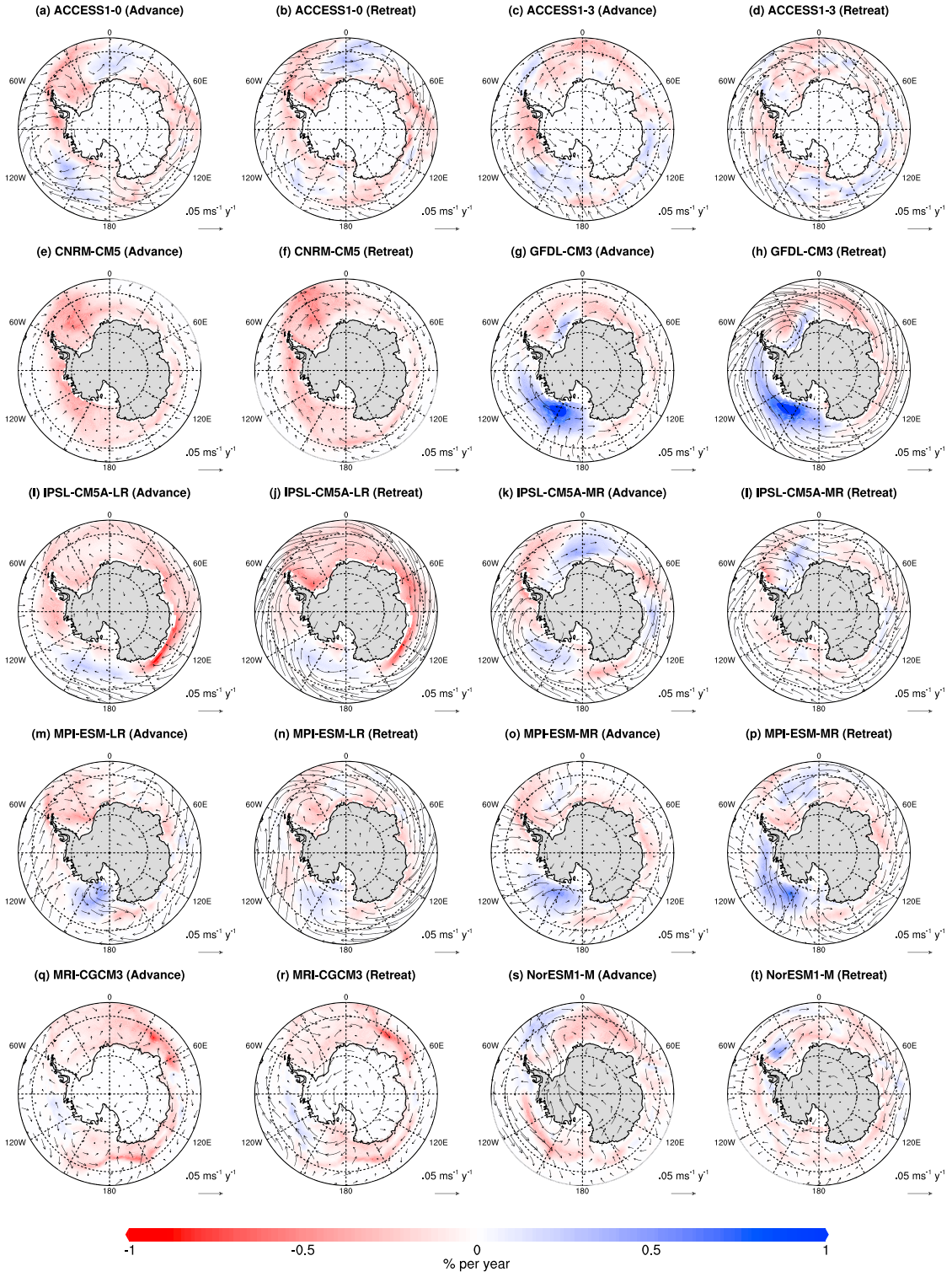

Figure 9. Trends of sea ice concentration (shading) and surface winds (arrows) from the ensemble mean of the historical experiment during the seasons of sea ice advance and retreat in (a, b) ACCESS1-0, (c, d) ACCESS1-3, (e, f) CNRM-CM5, (g, h) GFDL-CM3, (i, j) IPSL-CM5A-LR, (k, l) IPSL-CM5A-MR, (m, n) MPI-ESM-LR, (o, p) MPI-ESM-MR, (q, r) MRI-CGCM3, and (s, t) NorESM1-M. ACCESS = Australian Community Climate and Earth System Simulator; CNRM-CM5 = Centre National de Recherches Météorologiques Climate Model version 5; GFDL-CM3 = Geophysical Fluid Dynamics Laboratory Climate Model version 3; IPSL-CM5A-LR = Community Climate System Model and Institut Pierre Simon Laplace Low-Resolution model; IPSL-CM5A-MR = Community Climate System Model and Institut Pierre Simon Laplace Middle-Resolution model; MPI-ESM-LR = Max Planck Institute Earth System Low-Resolution model; MPI-ESM-MR = Max Planck Institute Earth System Mixed-Resolution model; MRI-CGCM3 = Meteorological Research Institute coupled global climate model; NorESM1-M = Norwegian Climate Center's Earth System Model.

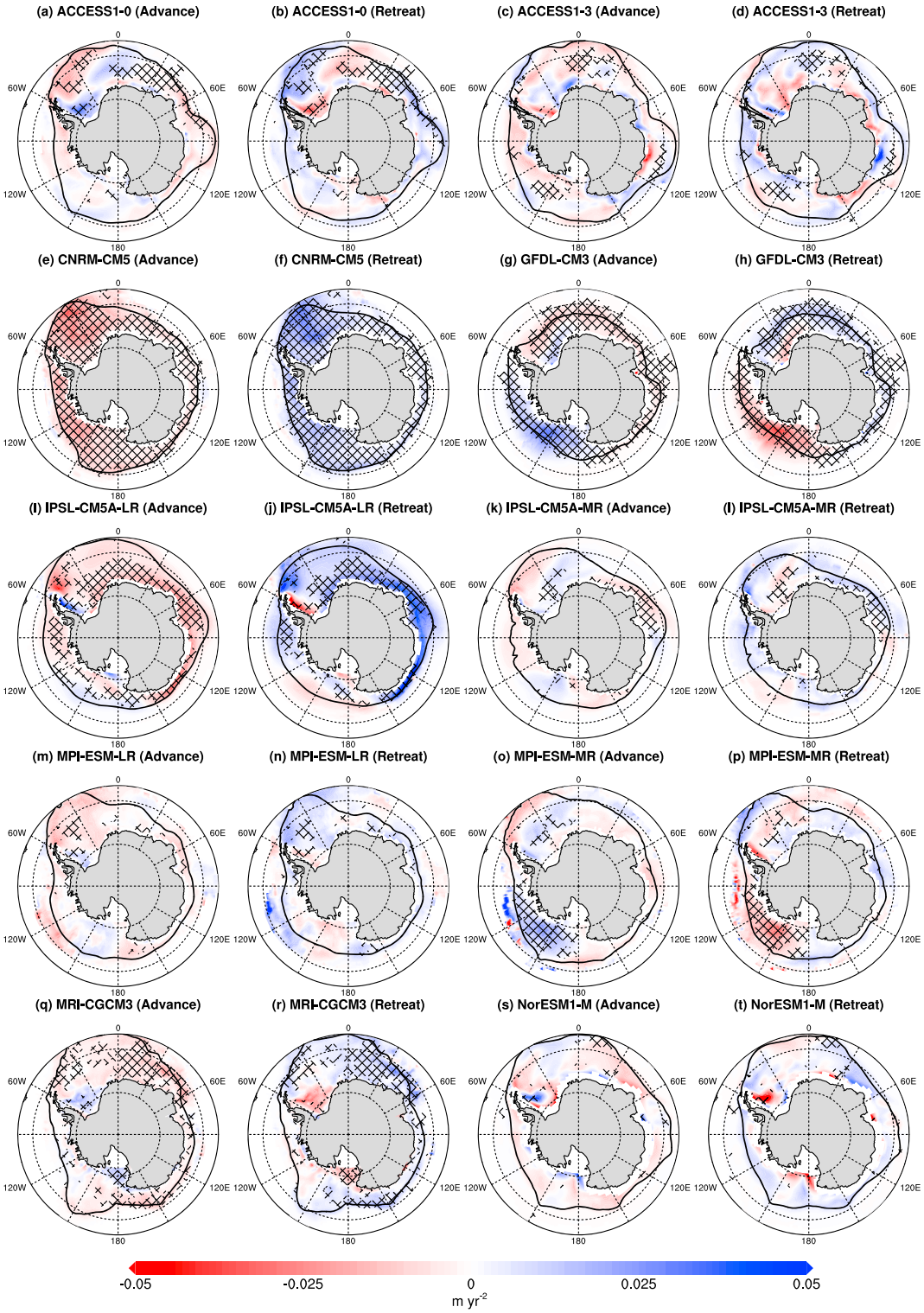

Figure 10. Trends of $\partial V/\partial t$ (shading; hatching shows trends that are statistically significant at the 95% confidence level) from the ensemble mean of the historical experiment and mean sea ice extent (thick black line) from the pre-industrial control experiment during the seasons of sea ice advance and retreat. ACCESS = Australian Community Climate and Earth System Simulator; CNRM-CM5 = Centre National de Recherches Météorologiques Climate Model version 5; GFDL-CM3 = Geophysical Fluid Dynamics Laboratory Climate Model version 3; IPSL-CM5A-LR = Community Climate System Model and Institut Pierre Simon Laplace Low-Resolution model; IPSL-CM5A-MR = Community Climate System Model and Institut Pierre Simon Laplace Middle-Resolution model; MPI-ESM-LR = Max Planck Institute Earth System Low-Resolution model; MPI-ESM-MR = Max Planck Institute Earth System Mixed-Resolution model; MRI-CGCM3 = Meteorological Research Institute coupled global climate model; NorESM1-M = Norwegian Climate Center's Earth System Model.

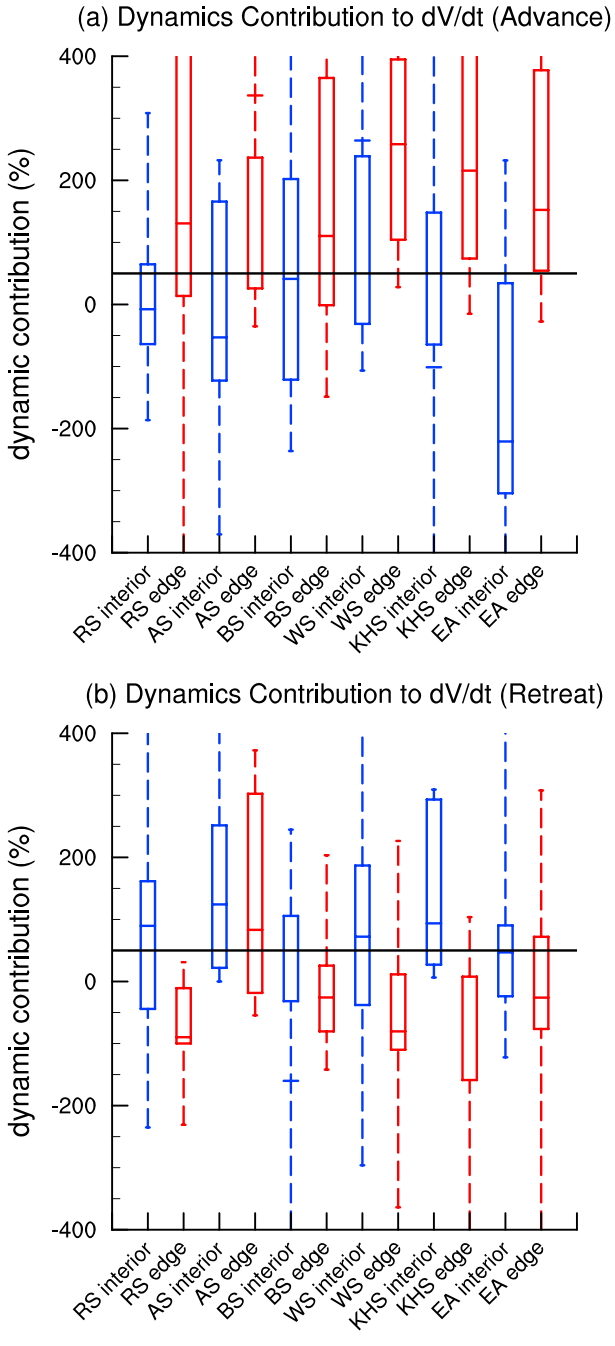

Figure 11. Relative magnitude of the dynamic contribution to trends of $\partial V/\partial t$ during advance (a) and retreat (b) in the Ross Sea (RS), Amundsen Sea (AS), Bellingshausen Sea (BS), Weddell Sea (WS), King Hakon VII Sea (KHS), and East Antarctic (EA) sectors at the sea ice interior (blue) and edge (red). Boxes show the 20–80% quartile range. Black line indicates 50% positive contribution to $\partial V/\partial t$; values above this line show sectors and seasons where dynamic processes dominate $\partial V/\partial t$, and values below show where thermodynamic processes dominate instead. Positive values indicate that the dynamic term contributes to the regional $\partial V/\partial t$ trend (i.e., for a negative $\partial V/\partial t$ trend, a negative dynamic term would be a positive percentage contribution).

interior, while the ice edge trends are largely dominated by dynamic processes. During retreat, thermodynamic processes dominate the ice edge in all sectors except the Amundsen Sea (Figure 11b). In the ice interior, dynamics dominate the majority of models in some sectors, while in others there is no clear dominant driver (Figure 11b).

The spatial patterns of the dynamic contributions to $\partial V/\partial t$ trends vary widely between the models (Figure 12). Importantly, the surface wind trends do not uniquely explain the intermodel spread of the dynamic contributions. While some models with weak wind trends also have weak dynamic contributions (CNRM-CM5 and MRI-CGCM3), GFDL-CM3 also has a weak dynamic contribution but some of the strongest wind trends of the models analyzed here. By contrast, NorESM1-M (Figures 9s and 9t) does not have particularly large trends in surface winds compared with other models, and yet the trends in sea ice dynamics are among the largest of the models in this study. Some models have regions where decreasing northward sea ice motion leads to a reduction in coastal divergence during advance, such as in the Weddell Sea in ACCESS1-0 (Figure 12a) and in the western Ross Sea in NorESM1-M (Figure 12s). This is in agreement with a recent study showing dynamically driven coastal thickening of sea ice during autumn (Holland, 2014).

The thermodynamic (e.g., cold- and warm-air advection, ocean heat, and snowfall) contribution to $\partial V/\partial t$ trends (Figure 13) also differs between the models. In 4 of the 10 models studied here (CNRM-CM5, GFDL-CM3, MPI-ESM-MR, and MRI-CGCM3), thermodynamic processes are generally much larger in magnitude than the dynamic term, particularly during retreat, and are strongly reflective of the trend patterns of $\partial V/\partial t$ (Figure 10). As we showed in Figure 8, these models have the smallest-magnitude mean sea ice flow regimes of the models considered in this study, suggesting a negative bias in sea ice velocity that has been shown to influence the timing of sea ice retreat (Lecomte et al., 2016). Trends in the thermodynamic contribution in the remaining models are much noisier than the corresponding $\partial V/\partial t$ trends, and in some regions, the magnitude of trends of thermodynamic processes are comparable in magnitude to trends of sea ice dynamics, suggesting that in these models, dynamic and thermodynamic processes influencing sea ice are more tightly linked.

A common theme among the models with comparable dynamic and thermodynamic contributions is a reduction in dynamic processes at the ice edge, accompanied by a reduction in sea ice melt during the retreat season. This is likely due to less ice presence in the marginal ice zone, most commonly in the Weddell and/or King Hakon VII seas and East Antarctica (e.g., Figures 9b, 9d, 9j, 9i, 10b, 10d, 10j, and 10i).

Studies have suggested that strengthening zonal winds in the sea ice zone can increase northward Ekman transport of cold surface water, and thus increase northward sea ice transport (Fan et al., 2014; Hall & Visbeck, 2002). Over time, however, the increased northward surface water transport leads to increased upwelling of relatively warm water from below the mixed ocean layer (Bitz & Polvani, 2012; Ferreira et al., 2015), which can enhance sea ice melt. Most of the models (ACCESS1-0, CNRM-CM5, GFDL-CM3, IPSL-CM5A-LR, MPI-ESM-LR, MRI-CGCM3, and NorESM1-M) have evidence of this process around East Antarctica, with decreasing sea ice along with intensified westerly wind trends.

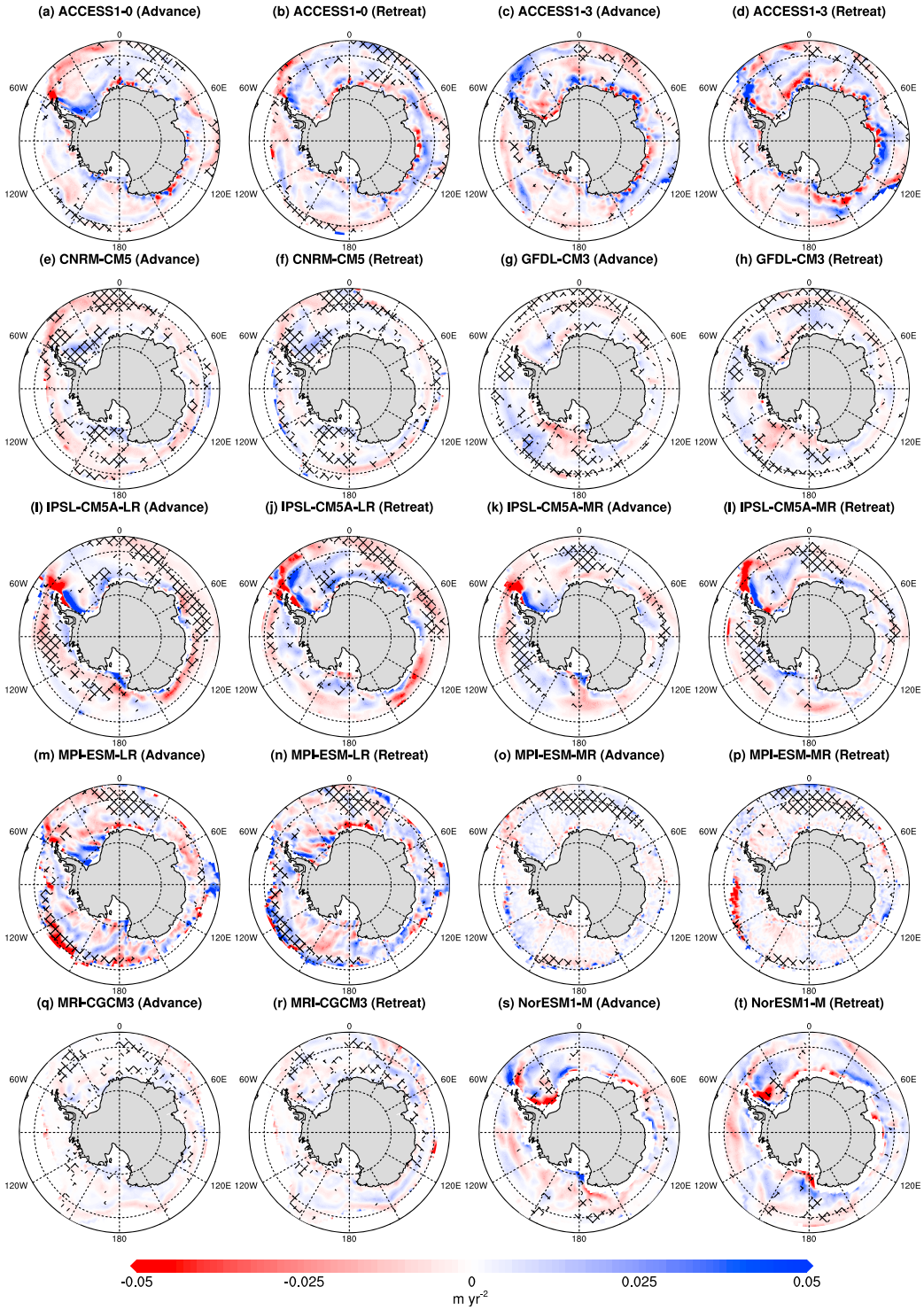

Figure 12. Trends of the dynamic contribution to $\partial V/\partial t$ (shading; hatching shows trends that are statistically significant at the 95% confidence level) from the ensemble mean of the historical experiment during the seasons of sea ice advance and retreat in (a, b) ACCESS1-0, (c, d) ACCESS1-3, (e, f) CNRM-CM5, (g, h) GFDL-CM3, (i, j) IPSL-CM5A-LR, (k, l) IPSL-CM5A-MR, (m, n) MPI-ESM-LR, (o, p) MPI-ESM-MR, (q, r) MRI-CGCM3, and (s, t) NorESM1-M. ACCESS = Australian Community Climate and Earth System Simulator; CNRM-CM5 = Centre National de Recherches Météorologiques Climate Model version 5; GFDL-CM3 = Geophysical Fluid Dynamics Laboratory Climate Model version 3; IPSL-CM5A-LR = Community Climate System Model and Institut Pierre Simon Laplace Low-Resolution model; IPSL-CM5A-MR = Community Climate System Model and Institut Pierre Simon Laplace Middle-Resolution model; MPI-ESM-LR = Max Planck Institute Earth System Low-Resolution model; MPI-ESM-MR = Max Planck Institute Earth System Mixed-Resolution model; MRI-CGCM3 = Meteorological Research Institute coupled global climate model; NorESM1-M = Norwegian Climate Center's Earth System Model.

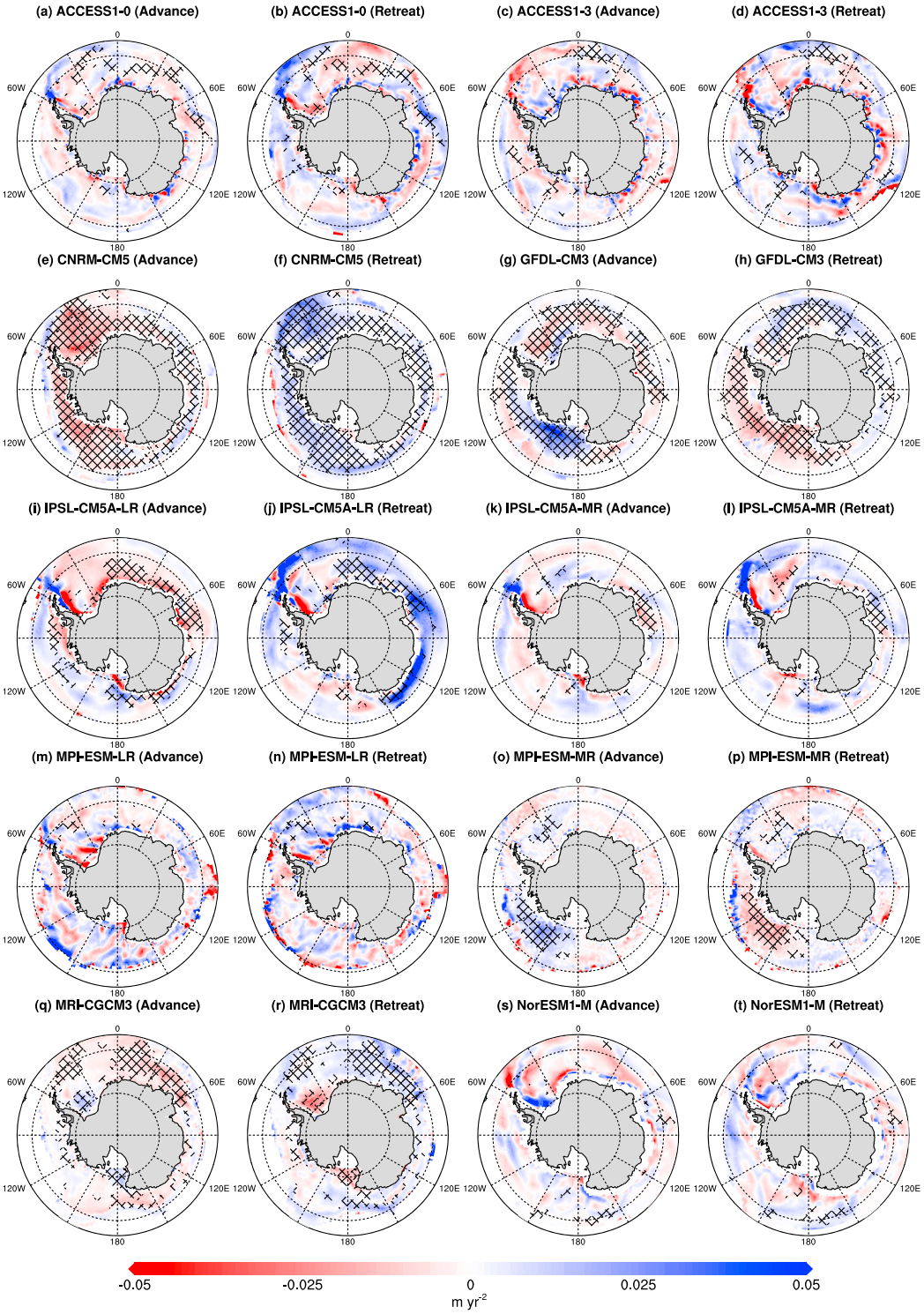

Figure 13. Trends of the thermodynamic contribution to $\partial V/\partial t$ (shading; hatching shows trends that are statistically significant at the 95% confidence level) from the ensemble mean of the historical experiment during the seasons of sea ice advance and retreat in (a, b) ACCESS1-0, (c, d) ACCESS1-3, (e, f) CNRM-CM5, (g, h) GFDL-CM3, (i, j) IPSL-CM5A-LR, (k, l) IPSL-CM5A-MR, (m, n) MPI-ESM-LR, (o, p) MPI-ESM-MR, (q, r) MRI-CGCM3, and (s, t) NorESM1-M. ACCESS = Australian Community Climate and Earth System Simulator; CNRM-CM5 = Centre National de Recherches Météorologiques Climate Model version 5; GFDL-CM3 = Geophysical Fluid Dynamics Laboratory Climate Model version 3; IPSL-CM5A-LR = Community Climate System Model and Institut Pierre Simon Laplace Low-Resolution model; IPSL-CM5A-MR = Community Climate System Model and Institut Pierre Simon Laplace Middle-Resolution model; MPI-ESM-LR = Max Planck Institute Earth System Low-Resolution model; MPI-ESM-MR = Max Planck Institute Earth System Mixed-Resolution model; MRI-CGCM3 = Meteorological Research Institute coupled global climate model; NorESM1-M = Norwegian Climate Center's Earth System Model.

4. Discussion and Conclusions

The 10 CMIP5 model configurations examined here are in good agreement about the dominant driver of mean sea ice volume change ($\partial V/\partial t$). At the ice edge, $\partial V/\partial t$ is dominated by dynamic processes during advance, and thermodynamic processes during retreat. In the sea ice interior, thermodynamics dominate in both advance and retreat.

However, the models disagree as to the dominant drivers of $\partial V/\partial t$ trends, with a large spread between the models, although at the sea ice edge $\partial V/\partial t$ trends tend to be dominated by dynamics during advance and by thermodynamics during retreat. In the interior, the opposite is true with the dynamic term tending to dominate the trends in retreat and the thermodynamic term tending to dominate in advance.

The spread of model trends shows that, as has been suggested for observations, there is likely no single physical process driving Antarctic sea ice trends (Holland, 2014); the dominant drivers are strongly dependent on region and model. This reinforces the conclusion of Kimura and Wakatsuchi (2011) that model performance should be assessed based on whether or not the model adequately represents the physical processes driving sea ice change. Examination of individual model patterns reveals that in the four models with the lowest-magnitude sea ice transport (CNRM-CM5, GFDL-CM3, MPI-ESM-MR, and MRI-CGCM3), sea ice trends are dominated by thermodynamic processes in the vast majority of sectors and seasons. In the remaining models, all of which have larger-magnitude mean sea ice mass transport, the dominant driver of $\partial V/\partial t$ trends is more spatially variable.

Importantly, although model bias in mean Antarctic sea ice can give insight into the magnitude of sea ice loss in response to anthropogenic forcing (Bracegirdle et al., 2015; Turner et al., 2013), our analysis demonstrates that sea ice concentration bias does not indicate the dominant processes driving sea ice trends in each model. MRI-CGCM3 has larger mean sea ice concentration and extent and yet is generally dominated more by thermodynamics than dynamics, whereas ACCESS1-0, ACCESS1-3, and NorESM1-M—all of which also have larger mean sea ice concentration and extent—show much large spatial variability in their dominant drivers. Conversely, IPSL-CM5A-LR and IPSL-CM5A-MR both have low mean sea ice concentration and extent and yet have large spatial variability as to which driver dominates.

In most of the models, mean sea ice dynamics play a strong role in the coastal zone, where changes to the easterly coastal winds that drive sea ice convergence can lead to dynamical ice thickening (Holland, 2014). This is particularly prevalent in models such as ACCESS1-0 and ACCESS1-3, which are known to have a positive bias in coastal sea ice convergence (Uotila et al., 2014). A common feature of several models, with both high and low mean sea ice, is large values of mean seasonal $\partial V/\partial t$ driven by thermodynamic processes at the ice edge across the Weddell Sea, which is a key process driving mean observed seasonal sea ice advance in this region in particular (Kimura & Wakatsuchi, 2011).

In several of the models, reduced northward transport of ice to the ice edge is associated with a reduction in sea ice melt. This has substantial implications for the simulation of ocean-sea ice interactions, as sea ice transport changes the relative location of brine rejection associated with sea ice production and surface freshening occurring during the sea ice melt (Haumann et al., 2016). The sea ice-related salinity budget around Antarctica moderates the simulation of Intermediate and Bottom Water, with substantial impacts for the ocean density structure and, subsequently, upper-ocean heat, carbon and nutrient transport (Abernathey et al., 2016; England, 1992; Haumann et al., 2016; Orsi et al., 1999; Pellichero et al., 2017; Rintoul & Garabato, 2013).

All models show a level of compensation in the thermodynamic contributions between the two seasons, where a positive trend during retreat is balanced by a corresponding negative trend during advance, and vice versa. For example, negative $\partial V/\partial t$ trends during advance are generally associated with negative thermodynamic trends, while positive trends of $\partial V/\partial t$ and thermodynamics during retreat imply a reduction in melting due to decreased availability of sea ice to melt during this season. Where $\partial V/\partial t$ is increasing, the reverse is generally true: the thermodynamic trends are negative during retreat and positive during advance, suggesting an enhanced freeze and melt cycle with greater ice presence during autumn and enhanced melt during spring. A similar phenomenon has been argued for in observed sea ice concentration trends (Holland, 2014), whereby trends originate during retreat, with compensating autumn trends being more closely linked to thermodynamic ocean-sea ice-atmosphere interactions than to zero-lag wind trends.

Positive trends in sea ice concentration and $\partial V/\partial t$ in GFDL-CM3, MPI-ESM-LR, and MPI-ESM-MR cannot be readily explained by wind trends alone. In these models, ocean changes may play a stronger role than the atmosphere in driving trends in some regions, as has previously been suggested for MPI-ESM-LR by Haumann et al. (2014).

There are several differences between our analysis of global coupled climate models and the observational analysis of Holland and Kwok (2012). We use a full sea ice budget while their analysis uses sea ice concentration, and we use ensemble mean trends, reducing noise in the results. Moreover, the timespan of the observational analysis in Holland and Kwok (2012) is 1992–2010, while our analysis encapsulates 1979–2005. The substantial difference between sea ice trends across the 1992–2010 timespan and the full passive microwave record from 1979 is highlighted in Hobbs et al. (2016). However, even using an extended observed sea ice motion data set spanning more than three decades, discrepancies are found between observed sea ice drift and reanalysis wind trends, which are either attributed to the limitations of current reanalysis products or remain as yet unexplained (Kwok et al., 2017).

While it is possible that the CMIP5 models are simply inadequately resolving dynamical processes that influence their sea ice budgets and processes, our results are consistent with a separate recent modeling study using reanalysis atmospheric boundary conditions showing that Antarctic sea ice trends may be driven largely by thermodynamics (Kusahara et al., 2017). It should be noted that the results of our study are based on relatively long timescales (seasons of 5–6 months) as well as large spatial scales, and the strength of the relative signals of the sea ice budget components in our analysis may prove to be different across higher temporal and spatial resolution data sets.

Furthermore, the overlap of the CMIP5 historical experiment (up to 2005) and the beginning of the satellite record (from 1979) produces a relatively short period for analysis, and internal variability therefore may contribute to the disparity between these models, as well as between models and observations. It has been shown that models not only overestimate internal variability in Antarctic sea ice during winter but also produce varying magnitudes of internal variability between seasons (Zunz et al., 2013). Averaging over the members for each model as we have done reduces some of the noise of internal variability; the number of members comprising the ensemble for each model is shown in Table 1. However, the regions of statistically significant trends (hatching in Figures 10, 12, and 13, calculated for trends in each individual ensemble member, then averaged across the members to produce an ensemble mean for each model) are not consistent between the models examined here. The lack of a clear consensus between the models on the spatial pattern of trend significance in $\partial V/\partial t$, dynamics, and thermodynamics could indicate the role of internal variability in the models in driving sea ice trends.

Our results cannot categorically conclude whether the relatively large contribution of thermodynamic drivers to trends of Antarctic sea ice in CMIP5 models compared to observational studies is correct or due to the poor representation of atmospheric and oceanic interactions with sea ice. However, in light of our results it seems justified to reexamine whether observed trends are indeed dominated by sea ice motion or whether the dynamical effects of wind stress play a smaller role than warm- or cold-air advection in driving Antarctic sea ice change than is currently presumed. The disparity between wind and sea ice trends in some of the models also suggest that ocean-sea ice processes may contribute strongly in driving changes to Antarctic sea ice and require further examination in global climate models.

Acknowledgments
The authors would like to thank Phil Reid and four anonymous reviewers for their thoughtful contributions to this article. Serena Schroeter was supported by an Australian Government Research Training Program Scholarship through the University of Tasmania/CSIRO Quantitative Marine Science Programme, and CMIP5 data management was supported by the Australian Research Council Centre of Excellence for Climate System Science. We thank the World Climate Research Programme's Working Group on Coupled Modeling and the climate modeling groups listed in Table for producing and making available CMIP5 model output (via https://cmip.llnl.gov/cmip5/data_portal.html). We thank the National Snow and Ice Data Center for access to passive microwave sea ice concentration data (via https://nsidc.org/data/NSIDC-0051), and the European Centre for Medium-Range Weather Forecasts for access to the ERA-Interim atmospheric reanalysis output (via http://apps.ecmwf.int/). For CMIP, the U.S. Department of Energy's Program for Climate Model Diagnosis and Intercomparison provides coordinating support and led development of software infrastructure in partnership with the Global Organization for Earth System Science Portals. This work was supported by the Australian Government's Cooperative Research Centres Programme through the Antarctic Climate and Ecosystems Cooperative Research Center (ACE CRC) and contributes to AAS Project 4116.

References

Abernathey, R. P., Cerovecki, I., Holland, P. R., Newsom, E., Mazloff, M., & Talley, L. D. (2016). Water-mass transformation by sea ice in the upper branch of the Southern Ocean overturning. *Nature Geoscience*, *9*(8), 596–601. https://doi.org/10.1038/ngeo2749

Bentsen, M., Bethke, I., Debernard, J., Iversen, T., Kirkevåg, A., Seland, Ø., et al. (2012). The Norwegian earth system model, NorESM1-M—Part 1: Description and basic evaluation. *Geoscientific Model Development Discussion*, *5*(3), 2843–2931. https://doi.org/10.5194/gmdd-5-2843-2012

Bi, D., Dix, M., Marsland, S. J., O'Farrell, S., Rashid, H., Uotila, P., et al. (2013). The ACCESS coupled model: Description, control climate and evaluation. *Australian Meteorological and Oceanographic Journal*, *63*(1), 41–64. https://doi.org/10.22499/2.6301.004

Bitz, C., & Polvani, L. M. (2012). Antarctic climate response to stratospheric ozone depletion in a fine resolution ocean climate model. *Geophysical Research Letters*, *39*, L20705. https://doi.org/10.1029/2012GL053393

Bitz, C. M., Gent, P. R., Woodgate, R. A., Holland, M. M., & Lindsay, R. (2006). The influence of sea ice on ocean heat uptake in response to increasing CO_2. *Journal of Climate*, *19*(11), 2437–2450. https://doi.org/10.1175/jcli3756.1

Bracegirdle, T. J., Stephenson, D. B., Turner, J., & Phillips, T. (2015). The importance of sea ice area biases in 21st century multimodel projections of Antarctic temperature and precipitation. *Geophysical Research Letters*, *42*, 10,832–10,839. https://doi.org/10.1002/2015GL067055

Comiso, J. C., Gersten, R. A., Stock, L. V., Turner, J., Perez, G. J., & Cho, K. (2017). Positive trend in the Antarctic sea ice cover and associated changes in surface temperature. *Journal of Climate*, *30*(6), 2251–2267. https://doi.org/10.1175/JCLI-D-16-0408.1

Dufresne, J.-L., Foujols, M.-A., Denvil, S., Caubel, A., Marti, O., Aumont, O., et al. (2013). Climate change projections using the IPSL-CM5 Earth System Model: From CMIP3 to CMIP5. *Climate Dynamics*, *40*(9–10), 2123–2165. https://doi.org/10.1007/s00382-012-1636-1

England, M. H. (1992). On the formation of Antarctic intermediate and bottom water in ocean general circulation models. *Journal of Physical Oceanography*, *22*(8), 918–926. https://doi.org/10.1175/1520-0485(1992)022<0918:OTFOAI>2.0.CO;2

Fan, T., Deser, C., & Schneider, D. P. (2014). Recent Antarctic sea ice trends in the context of Southern Ocean surface climate variations since 1950. *Geophysical Research Letters*, *41*, 2419–2426. https://doi.org/10.1002/2014GL059239

Ferreira, D., Marshall, J., Bitz, C. M., Solomon, S., & Plumb, A. (2015). Antarctic ocean and sea ice response to ozone depletion: A two-time-scale problem. *Journal of Climate*, *28*(3), 1206–1226. https://doi.org/10.1175/JCLI-D-14-00313.1

Goosse, H., Campin, J. M., Fichefet, T., & Deleersnijder, E. (1997). Impact of sea-ice formation on the properties of Antarctic bottom water. *Annals of Glaciology*, *25*, 276–281. https://doi.org/10.3189/S0260305500014154

Gordon, A. L. (1981). Seasonality of Southern Ocean sea ice. *Journal of Geophysical Research*, *86*(C5), 4193–4197. https://doi.org/10.1029/JC086iC05p04193

Griffies, S. M., Winton, M., Donner, L. J., Horowitz, L. W., Downes, S. M., Farneti, R., et al. (2011). The GFDL CM3 coupled climate model: Characteristics of the ocean and sea ice simulations. *Journal of Climate*, *24*(13), 3520–3544. https://doi.org/10.1175/2011jcli3964.1

Hall, A., & Visbeck, M. (2002). Synchronous variability in the southern hemisphere atmosphere, sea ice, and ocean resulting from the annular mode. *Journal of Climate*, *15*(21), 3043–3057. https://doi.org/10.1175/1520-0442(2002)015<3043:SVITSH>2.0.CO;2

Haumann, F. A., Gruber, N., Münnich, M., Frenger, I., & Kern, S. (2016). Sea-ice transport driving Southern Ocean salinity and its recent trends. *Nature*, *537*(7618), 89–92. https://doi.org/10.1038/nature19101

Haumann, F. A., Notz, D., & Schmidt, H. (2014). Anthropogenic influence on recent circulation-driven Antarctic sea ice changes. *Geophysical Research Letters*, *41*, 8429–8437. https://doi.org/10.1002/2014GL061659

Heuzé, C., Heywood, K. J., Stevens, D. P., & Ridley, J. K. (2013). Southern Ocean bottom water characteristics in CMIP5 models. *Geophysical Research Letters*, *40*, 1409–1414. https://doi.org/10.1002/grl.50287

Hobbs, W. R., Bindoff, N. L., & Raphael, M. N. (2015). New perspectives on observed and simulated Antarctic Sea ice extent trends using optimal fingerprinting techniques. *Journal of Climate*, *28*(4), 1543–1560. https://doi.org/10.1175/JCLI-D-14-00367.1

Hobbs, W. R., Massom, R., Stammerjohn, S., Reid, P., Williams, G., & Meier, W. (2016). A review of recent changes in Southern Ocean sea ice, their drivers and forcings. *Global and Planetary Change*, *143*, 228–250. https://doi.org/10.1016/j.gloplacha.2016.06.008

Holland, P. R. (2014). The seasonality of Antarctic sea ice trends. *Geophysical Research Letters*, *41*, 4230–4237. https://doi.org/10.1002/2014GL060172

Holland, P. R., & Kimura, N. (2016). Observed concentration budgets of Arctic and Antarctic sea ice. *Journal of Climate*, *29*(14), 5241–5249. https://doi.org/10.1175/JCLI-D-16-0121.1

Holland, P. R., & Kwok, R. (2012). Wind-driven trends in Antarctic sea-ice drift. *Nature Geoscience*, *5*(12), 872–875. https://doi.org/10.1038/ngeo1627

Hosking, J. S., Orr, A., Marshall, G. J., Turner, J., & Phillips, T. (2013). The influence of the amundsen-bellingshausen seas low on the climate of West Antarctica and its representation in coupled climate model simulations. *Journal of Climate*, *26*(17), 6633–6648. https://doi.org/10.1175/JCLI-D-12-00813.1

Jungclaus, J., Fischer, N., Haak, H., Lohmann, K., Marotzke, J., Matei, D., et al. (2013). Characteristics of the ocean simulations in the Max Planck Institute Ocean Model (MPIOM) the ocean component of the MPI-Earth system model. *Journal of Advances in Modeling Earth Systems*, *5*(2), 422–446. https://doi.org/10.1002/jame.20023

Kimura, N., & Wakatsuchi, M. (2011). Large-scale processes governing the seasonal variability of the Antarctic sea ice. *Tellus Series A: Dynamic Meteorology and Oceanography*, *63*(4), 828–840. https://doi.org/10.1111/j.1600-0870.2011.00526.x

Kusahara, K., Williams, G. D., Massom, R., Reid, P., & Hasumi, H. (2017). Roles of wind stress and thermodynamic forcing in recent trends in Antarctic sea ice and Southern Ocean SST: An ocean-sea ice model study. *Global and Planetary Change*, *158*(Supplement C), 103–118. https://doi.org/10.1016/j.gloplacha.2017.09.012

Kwok, R., Pang, S. S., & Kacimi, S. (2017). Sea ice drift in the Southern Ocean: Regional patterns, variability, and trends. *Elementa: Science of the Anthropocene*, *5*(0). https://doi.org/10.1525/elementa.226

Lecomte, O., Goosse, H., Fichefet, T., Holland, P., Uotila, P., Zunz, V., & Kimura, N. (2016). Impact of surface wind biases on the Antarctic sea ice concentration budget in climate models. *Ocean Modelling*, *105*, 60–70. https://doi.org/10.1016/j.ocemod.2016.08.001

Mahlstein, I., Gent, P. R., & Solomon, S. (2013). Historical Antarctic mean sea ice area, sea ice trends, and winds in CMIP5 simulations. *Journal of Geophysical Research: Atmospheres*, *118*, 5105–5110. https://doi.org/10.1002/jgrd.50443

Martinson, D. G. (1990). Evolution of the southern ocean winter mixed layer and sea ice: Open ocean deepwater formation and ventilation. *Journal of Geophysical Research*, *95*(C7), 11,641–11,654. https://doi.org/10.1029/JC095iC07p11641

Massom, R. A. (1992). Observing the advection of sea ice in the Weddell Sea using buoy and satellite passive microwave data. *Journal of Geophysical Research*, *97*(C10), 15,559–15,572. https://doi.org/10.1029/92JC01198

Massom, R. A., Stammerjohn, S. E., Lefebvre, W., Harangozo, S. A., Adams, N., Scambos, T. A., et al. (2008). West Antarctic Peninsula sea ice in 2005: Extreme ice compaction and ice edge retreat due to strong anomaly with respect to climate. *Journal of Geophysical Research*, *113*, C02S20. https://doi.org/10.1029/2007JC004239

Matear, R. J., O'Kane, T. J., Risbey, J. S., & Chamberlain, M. (2015). Sources of heterogeneous variability and trends in Antarctic sea-ice. *Nature Communications*, *6*, 8656. https://doi.org/10.1038/ncomms9656

Meier, W., Fetterer, F., Savoie, M., Mallory, S., Duerr, R., & Stroeve, J. (2015). *NOAA/NSIDC climate data record of passive microwave sea ice concentration, version 2*. Boulder, Colorado USA: National Snow and Ice Center. https://doi.org/10.7265/N55M63M1

National Academies of Sciences, Engineering, and Medicine (2017). *Antarctic sea ice variability in the Southern Ocean-Climate System*. Washington, DC: The National Academies Press.

Orsi, A., Johnson, G., & Bullister, J. (1999). Circulation, mixing, and production of Antarctic bottom water. *Progress in Oceanography*, *43*(1), 55–109. https://doi.org/10.1016/S0079-6611(99)00004-X

Pellichero, V., Sallée, J.-B., Schmidtko, S., Roquet, F., & Charrassin, J.-B. (2017). The ocean mixed layer under Southern Ocean sea-ice: Seasonal cycle and forcing. *Journal of Geophysical Research: Oceans*, *122*, 1608–1633. https://doi.org/10.1002/2016JC011970

Puri, K. (2012). The Australian Community Climate and Earth System Simulator, ACCESS: Scientific justification and options for system development. *Australian Meteorological and Oceanographic Journal*, *62*(4), 195–210.

Raphael, M. N., & Hobbs, W. (2014). The influence of the large-scale atmospheric circulation on Antarctic sea ice during ice advance and retreat seasons. *Geophysical Research Letters*, *41*(41), 5037–5045. https://doi.org/10.1002/2014GL060365

Rintoul, S. R., & Garabato, A. C. N. (2013). Dynamics of the Southern Ocean circulation. In *International geophysics* (pp. 471–492). Kidlington, Oxford UK: Elsevier.

Sallée, J. B., Shuckburgh, E., Bruneau, N., Meijers, A. J., Bracegirdle, T. J., & Wang, Z. (2013). Assessment of Southern Ocean mixed-layer depths in CMIP5 models: Historical bias and forcing response. *Journal of Geophysical Research: Oceans*, *118*, 1845–1862. https://doi.org/10.1002/jgrc.20157

Schroeter, S., Hobbs, W., & Bindoff, N. L. (2017). Interactions between Antarctic sea ice and large-scale atmospheric modes in CMIP5 models. *The Cryosphere*, *11*(2), 789–803. https://doi.org/10.5194/tc-11-789-2017

Shu, Q., Song, Z., & Qiao, F. (2015). Assessment of sea ice simulations in the CMIP5 models. *The Cryosphere*, *9*(1), 399–409. https://doi.org/10.5194/tc-9-399-2015

Taylor, K. E., Stouffer, R. J., & Meehl, G. A. (2009). A summary of the CMIP5 experiment design, PCDMI Rep, 33.

Taylor, K. E., Stouffer, R. J., & Meehl, G. A. (2012). An overview of CMIP5 and the experiment design. *Bulletin of the American Meteorological Society*, *93*(4), 485–498. https://doi.org/10.1175/BAMS-D-11-00094.1

Timco, G., & Frederking, R. (1996). A review of sea ice density. *Cold Regions Science and Technology*, *24*(1), 1–6. https://doi.org/10.1016/0165-232X(95)00007-X

Turner, J., Bracegirdle, T. J., Phillips, T., Marshall, G. J., & Scott Hosking, J. (2013). An initial assessment of antarctic sea ice extent in the CMIP5 models. *Journal of Climate*, *26*(5), 1473–1484. https://doi.org/10.1175/JCLI-D-12-00068.1

Uotila, P., Holland, P. R., Vihma, T., Marsland, S. J., & Kimura, N. (2014). Is realistic Antarctic sea-ice extent in climate models the result of excessive ice drift? *Ocean Modelling*, *79*, 33–42. https://doi.org/10.1016/j.ocemod.2014.04.004

Uotila, P., O'Farrell, S., Marsland, S. J., & Bi, D. (2013). The sea-ice performance of the Australian climate models participating in the CMIP5. *Australian Meteorological and Oceanographic Journal*, *63*(1), 121–143. https://doi.org/10.22499/2.6301.008

Voldoire, A., Sanchez-Gomez, E., Mélia, D. S., Decharme, B. Y., Cassou, C., Sénési, S., et al. (2013). The CNRM-CM5. 1 global climate model: Description and basic evaluation. *Climate Dynamics*, *40*(9–10), 2091–2121. https://doi.org/10.1007/s00382-011-1259-y

Yukimoto, S., Adachi, Y., Hosaka, M., Sakami, T., Yoshimura, H., Hirabara, M., et al. (2012). A new global climate model of the Meteorological Research Institute: MRI-CGCM3—Model description and basic performance. *Journal of the Meteorological Society of Japan*, *90A*(0), 23–64. https://doi.org/10.2151/jmsj.2012-A02

Zunz, V., Goosse, H., & Massonnet, F. (2013). How does internal variability influence the ability of CMIP5 models to reproduce the recent trend in Southern Ocean sea ice extent? *The Cryosphere*, *7*(2), 451–468. https://doi.org/10.5194/tc-7-451-2013